Neuromuscular connectomes across development reveal synaptic ordering rules

Yaron Meirovitch[1,*,+], Kai Kang[1,*], Ryan W. Draft[1,*], Elisa C. Pavarino[1], Maria Fernanda Henao Echeverri[1], Fuming Yang[1], Stephen G. Turney[1], Daniel R. Berger[1], Adi Peleg[1], Richard L. Schalek[1], Ju Lu[2], Juan-Carlos Tapia[1,3,+], Jeff. W. Lichtman[1,+]

1 Department.of Molecular and Cellular Biology and Center for Brain Science, Harvard University, Cambridge, MA 02138
2 Department of Molecular, Cell and Developmental Biology, University of California Santa Cruz, Santa Cruz, CA 95064
3 School of Medicine, University of Talca, Talca, Chile

* Equal Contribution
+ Corresponding Authors: yaron.mr@gmail.com; juantapia@utalca.cl; jeff@mcb.harvard.edu

Abstract

The connections between motor neurons and muscle fibers are dramatically reorganized in early postnatal life. This work attempts to better understand this synaptic rewiring by using a connectomic approach, i.e., tracing out all the connections between motor neurons and muscle fibers, at successive ages in a small mouse muscle. We reconstructed 31 partial-complete neuromuscular connectomes, using serial section scanning electron microscopy in a neonatal mouse and Brainbow-based and XFP-based fluorescent reconstructions in older animals. Our data included a total of more than 6000 neuromuscular junctions (NMJs), including complete connectomes from one newborn, seven developmental ages (P6-P9), and two adults. Analysis confirmed the massive rewiring that takes place as axons prune their motor units but add more synaptic areas at the NMJs with which they remain in contact. Interestingly, we found synaptic ordering rules that likely underlie this circuit maturation and yield the resulting adult neuromuscular pattern, as manifest in Henneman's size principle. In particular, by analyzing both the identities of axons sharing NMJs at developing ages and muscle fibers with multiple endplates, we found evidence suggesting an activity-based linear ranking of motor neurons such that neurons co-innervated the same endplates and same muscle fibers (if there were more than one endplate) when the axons were similar in activity and hence rank. In addition, this ranking provided a means for understanding action at a distance in which the activity at one neuromuscular junction can impact the fate of the axons at another junction at a different site on the same muscle fiber. These activity-dependent mechanisms provide insight into the means by which timing of activity among different axons innervating the same population of cells, that start out with nearly all-to-all connectivity, can produce a well-organized system of axons, a system that is necessary for the recruitment order of neurons during a graded behavior like muscle contraction.

INTRODUCTION

The orderly recruitment of motor neurons known as Henneman's size principle is a nearly universal property of motor action in vertebrates (Henneman 1957; Zajac and Faden 1985). During a muscle action, motor neurons that generate little force presumably because they innervate small numbers of muscle fibers (i.e. have small motor units) are activated first and if this is insufficient for the task at hand, are aided by the recruitment of progressively larger motor units. How this recruitment pattern comes into being is not known. This problem is further complicated by the fact that motor units are larger in early postnatal development and individual muscle fibers are multiply innervated due to the convergence of more than one motor axon at individual neuromuscular junctions (NMJs; also known as motor endplates). In adults, otherwise, each muscle fiber contains a single neuromuscular junction, generally located near the center of the fiber, and it is contacted by only one motor axon. Thus, both the fan-out of individual motor axons and the fan-in of multiple axons decreases as animals are first using their muscles in postnatal life. In addition, the axon that remains at each neuromuscular junction establishes many new synaptic contacts there, to more than compensate for the loss of other inputs. In rodents this synapse elimination is typically complete in the first several weeks after birth. To the best of our knowledge, a link between the size principle and synapse elimination has not previously been made.

This change in connectivity over early development raises a number of questions related to the size principle (Henneman 1957; Henneman and Olson 1965): 1) Are motor units distributed in size in early postnatal life or do the motor unit size differences emerge because of pruning? 2) Is developmental synapse elimination related in any way to the size principle? 3) What is the role, if any, of activity in establishing the size principle? One reason the latter question is of interest is that there are a number of lines of evidence that suggest that the outcome of synapse elimination is based on activity differences between axons that innervate the same muscle fiber (W. A. Harris 1981; Personius and Balice-Gordon 2001; Buffelli et al. 2002; Wyatt and Balice-Gordon 2003; Favero, Busetto, and Cangiano 2012). Because of the recruitment order, individual neurons will have activity patterns that are most similar to the axon recruited just before and just after them. We wondered if as synapse elimination removes axons from neuromuscular junctions the axons with the most similar activity patterns would coexist longer than the axons with very different activity patterns.

All of these questions require knowing the sizes and connectivities of all the motor neurons that innervate a muscle. In previous work we rendered all the axons that innervated a small muscle in the adult mouse (Lu et al. 2009). In the present work we have done the same type of dense reconstructions but now at multiple developmental ages. This connectomic approach was challenging because we needed to resort to serial electron microscopy for the youngest age studied (the day of birth, P0). At the end of the first postnatal week, we could use multicolor brainbow mice (Livet et al. 2007) with confocal microscopy and at later ages the preparation was large enough that single color transgenic XFP mice (Feng et al. 2000) sufficed to get a connectome.

The results provided evidence that the adult size principle has its origins in the earliest stages of postnatal development and perhaps even earlier but synapse elimination in postnatal life is also involved. We find that synapse elimination is more organized than was previously expected. In particular, as synapse elimination proceeds the remaining axons that stay at the junctions depict an ordered arrangement that is compatible with synapse elimination being driven by differences in the activity of motor axons based on their position in the recruitment order. Lastly, we found evidence of a different kind of natural synapse elimination in postnatal life: the

elimination of supernumerary endplates which we ascribe to activity based synapse elimination working over long distances.

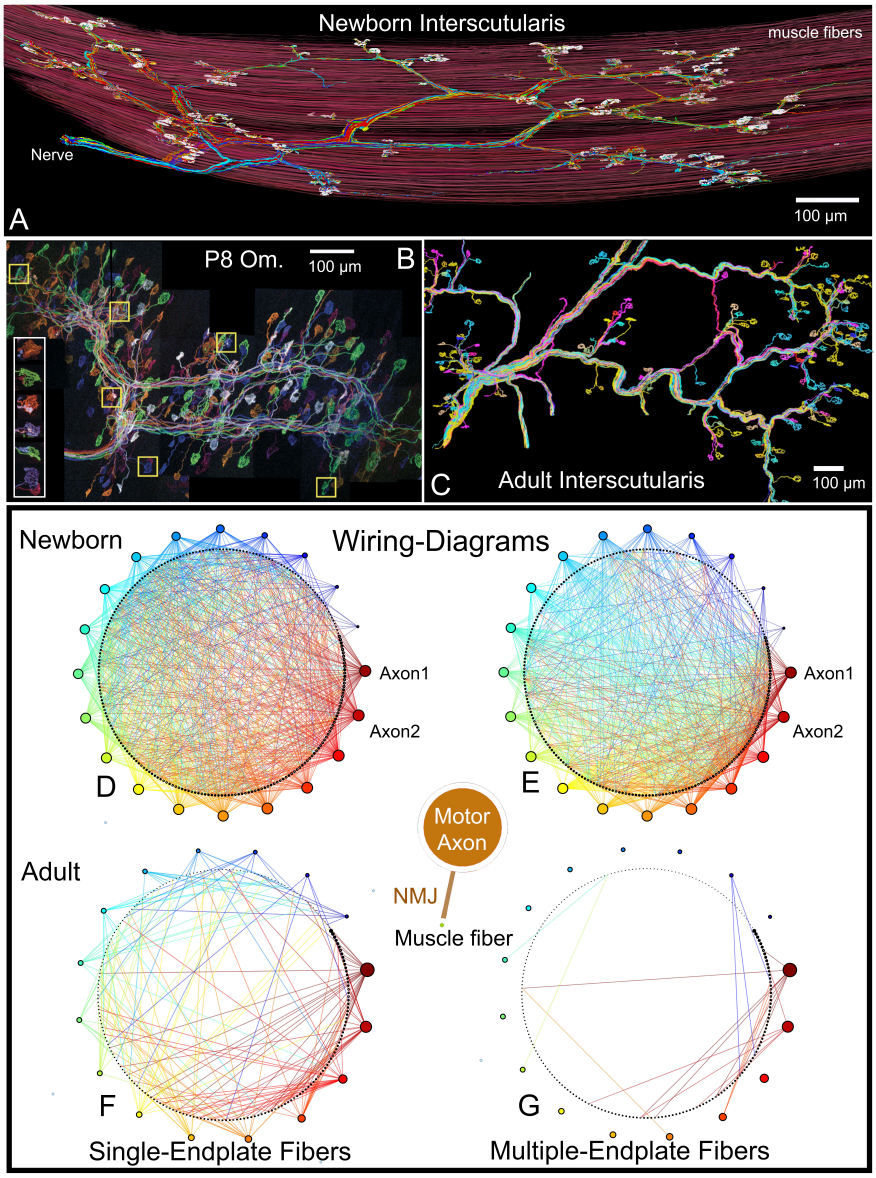

Figure 1. Muscle anatomy and wiring diagrams. A. A newborn interscutularis muscle and the innervating nerve reconstructed from volume electron microscopy (ssSEM) using 3D tracing aided by machine learning. Axons were colored according to their motor unit sizes (number of innervated muscle fibers). Red and blue for large and small motor units, respectively. Muscle fibers (red) and endplates (white) were individually reconstructed. **B.** One of the 7 developmental (P6-P9) neuromuscular connectomes reconstructed with the aid of brainbow labeling (Livet et al. 2007; Tsuriel et al. 2015). **C.** An adult interscutularis nerve and its entire axonal arborization reconstructed from high-resolution (138 nm/pixel) confocal stacks of XFP-based muscle using 3D tracing. **D-G**. Comparison between newborn and adult connectomes suggests massive rewiring: >1800 connections at birth and ~200 connections in adulthood; ~35% of the newborn muscle fibers possess multiple endplates, whereas ~94% of the adult muscle fibers possess a single endplate. The connections made on single-endplate fibers (SEFs, left) and multiple-endplate fibers (MEFs, right panels) are shown separately. The colored circles represent the motor axon's innervation while black circles indicate the target muscle fibers whose CSA is indicated by the corresponding size of the circle.

RESULTS

We compared the patterns of connectivity between lower motor neurons and muscle fibers in 31 individual muscles from 21 mice, ranging from newborn to adult. These datasets include a serial-section electron microscopy (EM) analysis of the entire connectional map (connectome) of the interscutularis muscle at birth (postnatal day 0, P0; Fig. 1A), brainbow-based reconstructions of omohyoid and lumbrical muscle connectomes at P6-9 (Fig. 1B), and two fluorescent protein (XFP)-based reconstructions of the interscutularis muscle connectome at P60 (Fig. 1C). For P3-5, P10-12, and P30, we reconstructed partial connectomes. As serial-section EM takes an extraordinary amount of time and effort, we only used it for the P0 reconstruction and obtained full connectomes at later ages with confocal microscopy instead. To aid in the segmentation of axons at P6-9, we bred brainbow mice and selected muscles with axons having distinct colors (see Methods). In the adult, monochromatic fluorescent protein expression suffices for tracing all the axons as shown previously (Lu et al. 2009). For many of the datasets we also analyzed the size and neuromuscular junction(s) of each muscle fiber.

The newborn and adult interscutularis connectomes differ in several ways

The neuromuscular wiring diagram is well known to change extensively in postnatal life (Purves and Lichtman 1980; Willshaw 1981; Bennett 1983; Hall and Sanes 1993; Sanes and Lichtman 1999). To better understand the extent of these changes we compared the neuromuscular connectomes at birth and in adulthood. We found three major differences. First, nearly 100% of newborn muscle fiber endplates received polyneuronal innervation, *i.e.*, innervated by more than one motor axon. However, the number of converging inputs on newborn endplates varied considerably (range: 1-13, mean: 6.53 +/- 2.17) (see also (Juan C. Tapia et al. 2012)). This ratio of convergence is greater than that reported by any previous electrophysiological study of newborn muscle; for example, 2-4 terminals per endplate in E21-P0 rat diaphragm (Redfern 1970; A. J. Harris and McCaig 1983), 3.1-3.5 in P4 lumbrical muscle (Jones et al., 1986) and 2-6 in P0 EDL (Balice-Gordon and Thompson, 1988). This discrepancy is consistent with the methodological limitations of measuring weak synapses by electrodes (Brown, Jansen, and Van Essen 1976; Bennett and Pettigrew 1974). By contrast, 100% of adult endplates were mono-neuronally innervated by a single axon. Second, 34.42% of the newborn muscle fibers possessed two or three endplate sites (multiple endplate fibers, MEFs), each of which received polyneuronal innervation. Twenty muscle fibers had two neuromuscular junctions (27.66%) and 6.76% (5 fibers) had three. The distance between these endplates was highly variable (range: 27.54 - 974.877 μm, mean 510 +/- 308 μm). By contrast, we found a smaller percentage (~6%) of fibers with two endplates in adult muscles (P30-P60; n=5) (MEFs range 1.4%-18.1% in individual muscles). One adult P30 muscle (of five studied) had only 3 fibers with multiple endplates; no adult muscle had any fiber with three endplates. Thus, during development both the number of axons per endplate (neuromuscular junction fan-in) and the number of endplates per muscle fiber decrease. Although it has been suggested that AChR plaques are removed from early prenatal muscles (Sanes and Lichtman 2001), our P0 data indicate that postnatal synapse elimination via wholesale endplate loss is also commonplace. Third, the motor unit size (i.e. the number of muscle fibers innervated by each motor axon) was far larger in the newborn: at P0, the motor unit size ranged from 13-120 muscle fiber targets per axon (average 91.65 +/- 32.42) whereas in adult (P60) muscles, the average motor unit size was 6.5 fold smaller (average 14.058 +/- 7.97, range: 3-39; n=2 connectomes). At both ages, we saw considerable variability in the sizes of the ensemble of motor units that innervated the muscle. In adults, motor unit size is thought to be related to the types of motor neurons that activate distinct types of muscle fibers (e.g., fast vs. slow muscle fibers (Burke, Levine, and Zajac 1971)).

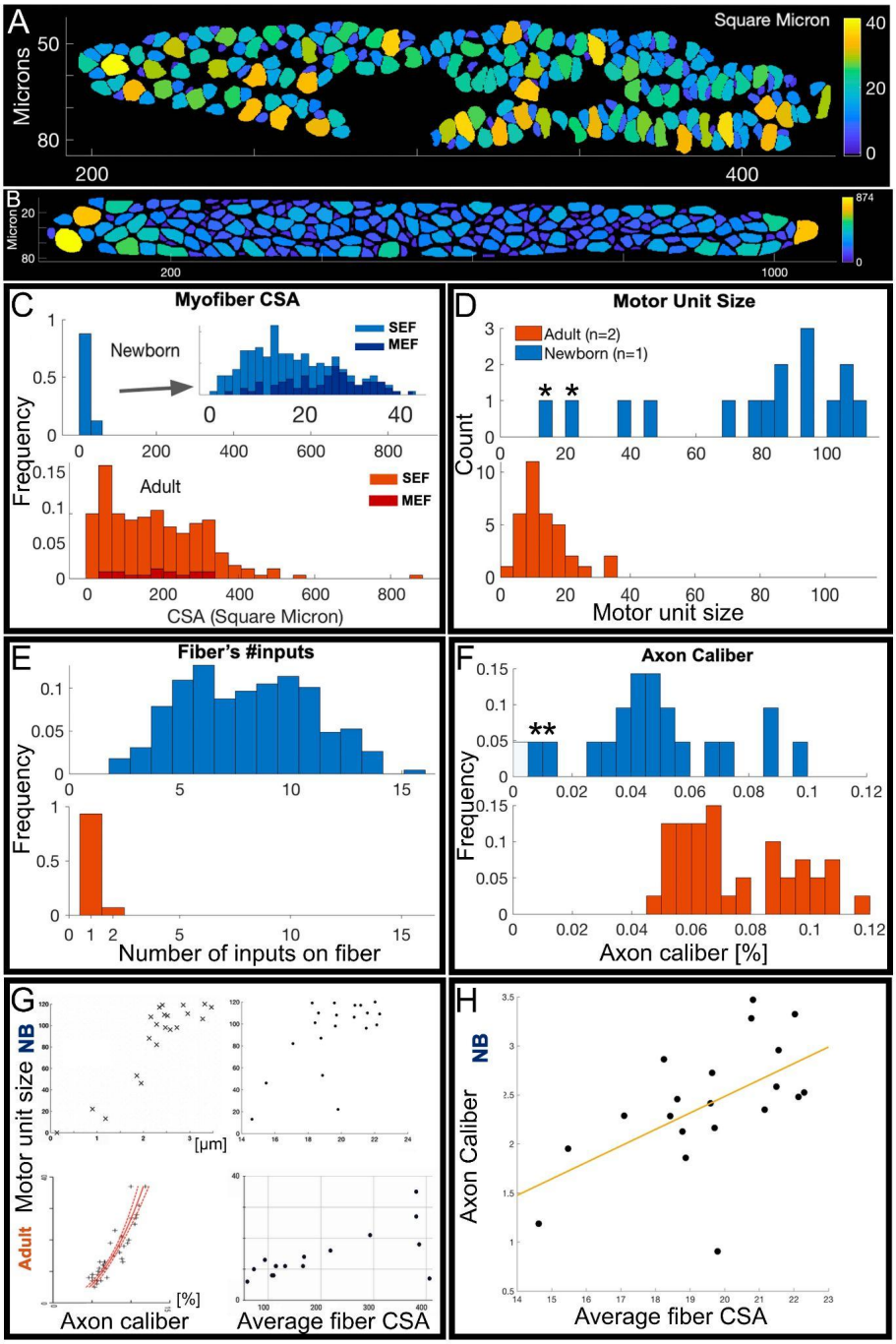

Figure 2. A size correlation between axons and their innervation targets from birth to adulthood. A-B. Transverse sections of a newborn (**A**) and an adult (**B**) interscutularis muscle. Patches represent individual muscle fibers colored by Cross-Sectional-Area (CSA). **C.** Newborn muscle fibers are ~10% the size of adult muscle fibers. At birth multiple-endplate fibers (MEF) are larger than single-endplate fibers (SEF); this size difference disappears in adulthood. **D.** The motor unit size drastically decreases from birth to adulthood and the shape of the distribution nearly flips. Due to size constraints, the two small motor units (marked by asterisks) cannot mature into the large motor units in the adult. **E.** The number of distinct axonal inputs onto individual muscle fibers is highly variable at birth (2-15) and reduces to one or two inputs in the adult for SEFs and MEFs, respectively. **F.** Axonal calibers normalized to the total area in a cross section of the nerve. Unlike adult axons, several newborn axons are extremely small compared to the entire population. **G-H.** Axonal calibers, motor unit sizes, and the average size of innervated muscle fibers are all correlated both at birth (NB) and in adulthood, suggesting that features of Henneman's size principle (Henneman 1957) start to emerge in perinatal life.

The variability in motor unit sizes in the newborn was unexpected, perhaps implying that even at birth motor axons are heterogeneous. For example, we found that at birth it was already clear that the smallest motor units could not give rise to the largest motor units in the adults because even before pruning they innervated fewer muscle fibers than the largest adult motor units (see Fig. 2D). Thus, there is already non-uniformity of motor units prior to the phase of massive synapse elimination. This conclusion is buttressed by the finding that the smallest motor units in the P0 muscle were axons with the smallest calibers (Fig. 2F).

From birth to adulthood synapses are extensively eliminated from muscle fiber endplates and, as already mentioned, even entire endplates are removed. However when we counted the numbers of muscle fibers and motor axons (5 muscles and 3 nerves at P0 and 5 muscles and 2 nerves in adults), we found that the total numbers of muscle fibers (P0: 222-270; adults: 205-254 muscle fibers) and the total number of motor axons (P0: 16-20; adults: 16-18 motor axons) do not differ substantially across age. This invariance in the number of pre- and postsynaptic cells allows us to directly compare the pattern of innervation from birth to adulthood. As described above, the larger motor units, the multiple innervation of endplates, and the existence of multiple endplates on single muscle fibers allows the perinatal connectivity to approach an all-to-all wiring diagram. Indeed, the total amount of possible connections between motor axons and muscle fibers was about 40% (1833 connections) of the theoretical maximum (i.e., dense connectivity with 240*20=4800 connections). This is starkly different from the adult neural organization wherein only ~6.13% (i.e., ~6-fold fewer) of the potential connections between motor axons and muscle fibers exist (i.e., sparse connectivity).

Despite the greater fan-in (neuromuscular junction input convergence) and fan-out (muscle fiber target divergence) of motor innervation in the newborn muscle, the axons do not distribute their innervation uniformly at random amongst the muscle fibers. Rather, at birth both the muscle fibers and the motor axons show bias in terms of the connections they establish. There are three lines of evidence that show this non-randomness. First, the sizes of motor units were highly variable which was not expected from the total number of synaptic connections that are present in the newborn muscle (the large std of motor unit sizes, 32.4269, is unlikely to derive from a random distribution, estimated from a collection of random connectomes with the fiber's number of inputs as in the data; $p<1/10^5$; see Methods). For example, several motor units were 2-6 fold larger than other motor units. In particular, 11 motor units each innervated at least 100 muscle fibers whereas 4 motor units each innervated only 13-53 muscle fibers. Hence, some motor neurons were unexpectedly larger (or smaller) than others. Second, the number of converging inputs on muscle fibers was also highly variable and inconsistent with a uniform distribution ($p<1/10^5$ using random connectomes with motor units as in the data). Some fibers received 3 axonal inputs while others received 16 axonal inputs. Hence, some muscle fibers receive significantly more (or less) converging inputs. The number of inputs appears to be directly related to the cross-sectional area of the innervated muscle fiber (Fig. S1A; $p<0.001$). Moreover, most of the large motor axons showed a preference for innervating larger caliber muscle fibers (in total 10/20 axons showed this preference $p<0.001$ as in Fig. S1B; group selectivity compared against random connectomes was $p<0.001$; see Methods). Third, we discovered that the motor unit size, the average muscle fiber caliber (cross-sectional area; CSA), and the motor axon caliber were correlated. In newborns, these three parameters, at the muscle entrance, all covaried (see correlations in Fig. 2G/H; pearson correlation between axon caliber and motor unit size $r=0.89$ $p<1/10^7$; axon caliber and average myofiber CSA $r=0.556$ $p=0.0108$; average myofiber CSA and motor unit size $r=0.629$ $p=0.0029$). In particular, the smallest motor units had the smallest axonal calibers and tended to innervate the thinnest muscle fibers, and vice versa for the largest motor units. This motor unit size-related pattern of

innervation is analogous to that in adult muscles (including in this muscle (Lu et al. 2009)), in which the motor unit size is correlated with the caliber of each motor axon at the entrance of the muscle. This correlation is part of the underlying reason for the orderly recruitment of progressively more powerful motor units, known as the size principle (Henneman 1957). It was unexpected that size principle-like features would exist at birth and raises the possibility that axonal activity patterns are already heterogeneous in the newborn. These results suggest that neonatal muscle fiber and axonal properties are heterogeneous and are manifested in the newborn innervation pattern. However, we could not detect other ultrastructural features that contrived with muscle fiber caliber such as sarcomere spacing, z-line thickness, and nuclear domain sizes, features that do differentiate muscle fiber types in adult muscles (Tseng, Kasper, and Edgerton 1994; Granzier, Akster, and Ter Keurs 1991). Rather these features were unimodally distributed among the muscle fibers. Nonetheless, newborn muscle is populated by a heterogeneous population of both motor axons and muscle fibers.

Given that muscle fibers are innervated by multiple axons in the neonate, the heterogeneity in the innervation patterns we just described suggests that “alike” axons might co-innervate corresponding muscle fibers to a greater degree than expected by chance. We therefore assessed whether certain pairs of axons tended to share targets to a greater degree than expected by chance (see Methods). In particular, we calculated the probabilities for observing the number of co-innervated muscle fibers between each pair of motor axons (under the assumption that each axon innervates each muscle fiber with equal probability independent of other axons; see Methods). We found that in the newborn connectome many axonal pairs co-innervated a significantly larger number of muscle fibers than expected by chance (innervation estimated by assuming a random innervation model based on the motor unit sizes and number of muscle fibers, 2000 random connectomes; $p<0.001$, see Methods). Interestingly, some pairs exhibited significant avoidance of innervating the same muscle fibers ($p<0.001$). This organization of motor axons based on the targets they share, or avoid, indicates that the innervation pattern of axons is not random and rather reflects, minimally, developmental “variation” between motor neurons (see SI for comparison against the axon arbors’ topography). However, neither the similarity nor the mutual avoidance in innervation was absolute: no two axons had exactly the same repertoire of muscle fiber targets; conversely, pairs of axons always shared some muscle fibers. This pairwise analysis implies that there is some pattern of innervation but this analysis was insufficient to reveal the actual pattern.

Ordered pattern of innervation in newborn

We set out to examine if the nonrandom innervation between motor axons and muscle fibers was part of a more global connectional pattern. To search for such a pattern, we transformed the pairwise co-innervation network of axons into a graph, in which each node represents one motor axon, and each edge corresponds to a pair of axons co-innervating significantly more muscle fibers than expected by chance. We then weighted these inter-axonal edges by the degree to which they deviated from chance. This approach allowed all axons to be normalized to the same scale independent of their sizes. To visualize this network we graphed it in 2 dimensions as a series of graded springs (Morgan et al. 2016). See for example that neurons that co-innervated significantly more muscle fibers than expected by chance were pulled more closely together. Qualitatively, this axon network appeared elongated in one direction (Fig. 3 all panels). We therefore wanted to determine if this elongation property would also be evident in random axonal networks that are constrained by the same fan-in and fan-out statistics of the motor axons and muscle fibers found at birth (i.e., a so-called “configuration model”; (Newman 2018)). We simulated n=500 connectomes based on the configuration of the newborn connectome and for each such random connectome we computed a metric of network elongation (see Methods). We discovered that the P0 connectome is more linear (elongated) than would be expected by chance ($p<0.04$). This elongation has the

interesting implication that neuronal tendencies to co-innervate the same muscle fibers are arranged in some kind of ordered gradient. For example, in Fig. S2A axon 1 and 2 co-innervate 45 muscle fibers. The thick line between them means that this result strongly deviates from chance. Motor axon 1 shares innervation on 13 muscle fibers with motor axon 13; this is also highly significant given the small size of axon 13's motor unit (22 muscle fibers). Axon 13 shares 14 muscle fibers with motor unit 14 - also a highly significant result. Axon 14 shares 49 muscle fibers with axon 15 - also a significant result. Axon 15 is at one side of a set of motor axons that share a significant number of muscle fibers; it shares significant connections with 4 of these bunched clusters of motor units (axons 11, 17, 19, and 21). On the other side of this cluster of axons there is motor axon 18 that shares a significant number of muscle fibers with 5 motor axons in the cluster (Axons 4, 9, 16, 19, and 21) and one motor axon to its right (Axon 5). Both axons 5 and 18 share a significant number of targets with axon 6 at the end of the order. The important point of the arrangement is that with exception of the clustered motor units, axons seem to have strong preferences for just a few motor units and these motor units have strong preferences for a slightly shifted small set of motor units. It is somewhat akin to the likelihood of a person talking to their immediate neighbors on a street. Each person's house is uniquely situated so its immediate neighbor houses are different. We thus termed this elongation a "linear order of co-innervation".

We discovered that the observed linear order of neurons was related to a property of the muscle fibers. As already mentioned (Fig. 2), motor unit size was correlated with the CSA of the muscle fibers within the motor unit. In terms of the linear order, we found that motor units that preferentially incorporated muscle fibers with large CSA were located close to the middle of the linear order (i.e. where the cluster of motor units resides in Fig. 3A and Fig. S2C-D). In contrast, axons without preference for large muscle fibers were at the edges (poles) of the linear order (Fig. S2C-D). Most axons at the periphery seemed to be sampling from both small and large muscle fibers, except one axon that appeared to be specific to thin muscle fibers. Thus motor axons that are specific to larger fibers share more targets with other axons of their kind. Hence, the linear order pattern is not an emergent property of random networks and reflects some of the specificities between newborn motor axons and muscle fiber targets that exist in the newborn's connectome.

The adult muscle connectivity does not develop from the newborn muscle by random synapse elimination

The innervation pattern of muscle fibers in the newborn indicates that to some degree at least the connectivity of motor axons is arranged in an ordered system. In addition, the largest motor units have the largest axon calibers and show a tendency to innervate muscle fibers that also have the largest CSAs. These tendencies potentially prelude the size principle organization observed in the adult muscle, where adult axons and muscles are organized by recruitment order, i.e. the largest caliber axons (which have the largest motor units) tend to innervate the muscle fibers with largest CSA and are recruited last. Because the connectivity is much more extensive in newborns (~10x) we asked if the adult connectivity pattern may emerge from the newborn connectome by random pruning or a more specific refinement. We found that the distributions of motor unit sizes in the newborn and in adults (n=2 and n=6 from (Lu et al. 2009) are not scaled versions of one another: scaling the newborn histogram to match the average motor unit of the adult connectome resulted in a difference of 16 targets between the 95-percentile unit of the scaled newborn (14 targets) and that of the adult (30 targets), and similarly scaling the newborn distribution to match the 95-percentile of the adult resulted in a gap of 14 targets between the average motor unit sizes (see SI for more exhaustive comparison of the histograms). This result in and of itself does not resolve the role of neonatal pruning because some muscle fibers are already non-randomly innervated by more axons. We thus modeled the outcome of a gradual and random elimination of synapses from

the newborn connectome to see whether it leads to the adult connectome. We found that the simulated adult connectomes arising from random synaptic pruning have significantly different motor unit size ranges, mean sizes and variance. Notably, the largest motor units in the actual data are far larger than the random elimination model predicts (estimated $p<0.01$ - zero occurrences in 1000 randomly produced developing connectomes with the starting point taken from the P0 connectome; median 20, mean 20.088 +\- 2.0466). Hence, although the wiring between motor axons and muscle fibers shows some level of specificity at birth, this pattern is not sufficient to generate the adult connectome.

The linear order after birth

In the first several postnatal weeks the connectivity of muscles changes dramatically as axonal branches are pruned (Purves and Lichtman, 1980; Brown et al., 1976). This pruning reduces the number of muscle fibers that are shared between motor units. To determine if certain cohorts of motor neurons remained co-innervated longer (i.e., present at later stages) compared to others, we sought to reconstruct the muscle at later points in development, when a great deal of elimination had occurred but some multiple innervation remained. At time points near the end of development (P6-P9), reconstructing an entire muscle by serial EM becomes impractical due to its significantly increased physical size, so we opted for the brainbow transgenic labeling strategy, which provides sufficient resolution under the confocal microscope at this age. As the expression of the brainbow transgenes was weak in rostral muscles including the interscutularis at P6, we looked at connectomes at P6-9 in several small and more caudally located muscles in the neck (omohyoid) and the forepaw (lumbrical). We analyzed seven connectomes: four omohyoid (OM 1-4) and three lumbrical muscles (Lum 1-3). To assess the linear order, we produced networks whose edge length represent the attraction (short edge) and repulsion (long edges) between motor axons, as done for the newborn connectome. A linear order emerges in six muscles (4 of 4 omohyoid and 2 of 3 lumbrical muscles), suggesting that it is not a unique property of the interscutularis muscle. The only muscle that did not show a linear order (Lum 2) was in an advanced stage of synapse elimination, with 73.48% of the endplates already singly innervated, and it did show an overall co-innervation pattern beyond the chance level ($p<0.01$; Monte Carlo test measuring the total amount of sharing). One muscle presented a perfect linear order in terms of the nominal numbers of shared targets between motor axons (Fig. 3B and Fig. 5 and Discussion). Hence, the linear order does not become weaker after the first stage of the massive postnatal synapse elimination. This suggests that motor axon synapses are progressively eliminated according to innervation tendencies that already appear at birth. In addition, these findings suggest that motor axon synapses are eliminated based on developmental properties of motor neurons and muscle fibers, rather than based on stochastic processes that are independent of cell to cell interactions. This also raises the possibility that to some extent the outcome of synapse elimination could be anticipated from the earlier wiring diagrams (andthe linear order). For example, it is possible that the set of muscle fibers co-innervated by two axons beyond chance will maintain this innervation for a longer period while some of the other axons innervating these fibers will retract. This hypothesis posits that axons close to each other in the linear order later in development would be close to each other in the linear order before the first step of massive synapse elimination as well. Indeed, if such specificity of elimination exists the linear order will continue to hold even after the massive elimination. Finally, this raises the question whether the linear order continues into adulthood which can be answered only in the presence of adult multiply innervated fibers.

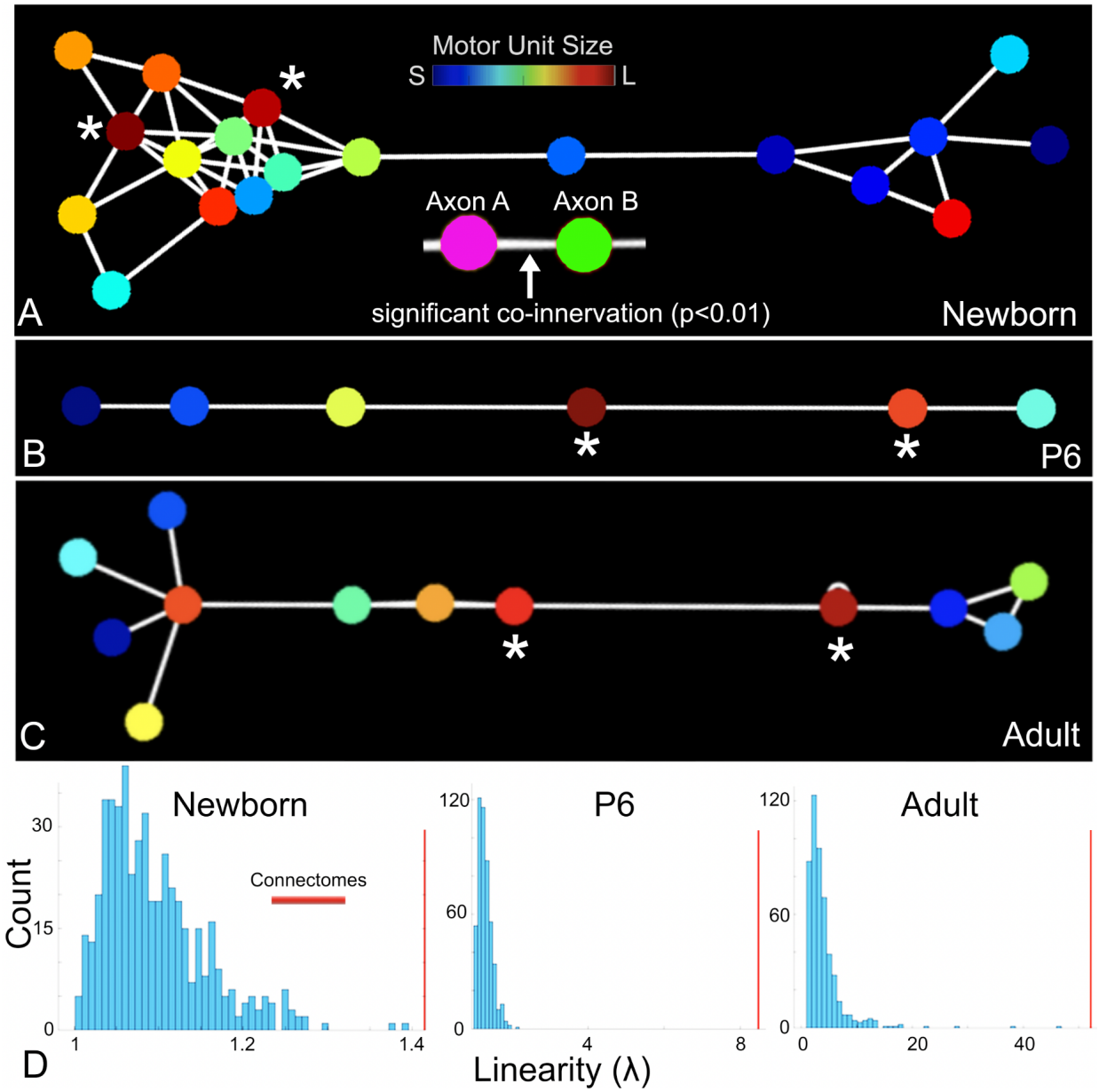

Figure 3. Linear order of axonal networks across maturation. A-C. The nodes in the graph representation correspond to axons whereas edges represent the number of shared targets between pairs of motor units. A pair of axons are connected by an edge if they co-innervate significantly more targets than expected by chance (A-B). The edge length represents the likelihood to observe the actual number of shared targets under the assumption of independent, uniform random innervation (short edges for excessive shared innervation). Nodes are positioned by an optimal 2-dimensional embedding using a spring-force algorithm (Fruchterman and Reingold 1991). The linearity within these axonal graphs (**λ**) was measured at P0, P6-P9 (n=7), and P60 (n=2) by comparing its elongation (eccentricity of the scattered nodes) to that of random connectomes with the same number of axons, fibers and motor unit sizes. The ability to embed the networks in 2D and obtain a large elongation index indicates that axons are rankable such that an axon's innervation proclivities were most similar to the axons on either side of it in the linear ranking. The two largest motor units are marked with asterisks. **D.** All three connectomes show elongation of the axonal network significantly beyond that of a random network (p<0.01). The red vertical lines indicate the elongation of the biological connectomes, compared against random size-matched connectomes.

Evidence of ordered innervation in adult muscles: multiple endplates on muscle fibers

At developmental ages, we inferred graded specificities of motor units for muscle fibers by virtue of the extensive co-innervation of muscle fibers by shifting subsets of motor neurons. As most adult muscle fibers are innervated by single axons at their solitary neuromuscular junctions, one cannot directly relate the developmental target-sharing to their adult state of innervation. However, as already mentioned above the adult interscutularis muscle retains a small number of multiple-endplate muscle fibers (MEFs). This number is ~6-fold fewer than the number of fibers with two or more neuromuscular junctions at birth. Hence, the developmental phase of synapse elimination both reduces the number of motor axons per endplate and the number of endplates per muscle fiber. We examined whether the remaining MEFs provide a link to the developmental ordering phenomena and the ultimate adult pattern of innervation (i.e. the size principle). Using confocal fluorescence microscopy in transgenic mice that express fluorescent protein in all motor axons (see Methods), we reconstructed the full connectomes of two adult interscutularis muscles including the neuromuscular junction sites (sometimes multiple), the axonal identities, and the CSA of each muscle fiber.

The two adult muscles were similar: muscle A was innervated by 18 axons and possessed 235 fibers and muscle B was innervated by 16 axons and possessed 217 muscle fibers. The number of MEFs was 13 in muscle A (5.53%) and 16 in muscle B (7.37%). The endplates on these MEFs were singly innervated as were the solitary endplates on the rest of the muscle fibers. In total, 26 endplates in muscle A (10.48%) and 32 endplates in muscle B (13.73%) were located on MEFs. Twelve of the 18 axons (66.67%) innervating muscle A innervated at least one endplate on MEFs, and seven of the 16 axons (43%) in muscle B innervated at least one endplate on MEFs. Interestingly the connectivity of MEF-innervating axons was unlikely to have occurred by chance. For example, in 4 cases in the 2 muscles the same axon innervated both neuromuscular junctions on the same muscle fiber. Furthermore, there were 6 instances in the two muscles where the same pair of axons co-innervated more than one MEF. In muscle A, only two MEFs were mono-neuronally innervated, which is not an unlikely event to occur by chance, but as we show below these pairs of co-innervating axons were ordered linearly, consistently with connectomes at younger ages. In muscle B, 6 MEFs received identical axonal inputs ($p<0.032$). There were even two cases where the same axons innervated 2 endplates on two different muscle fibers. This strong tendency of pairs of axons to co-innervate endplates on adult MEFs is consistent with the tendency of axons to repeatedly co-innervate the same endplates in younger age (as described above). All of these suggest that the identity of the axons in the adult that are co-innervating the same muscle fibers are associated with each other and are not drawn from a random distribution of axon pairs. As described earlier, all of these patterns are central features of the connectivity at birth and at P6.

The extra sharing as indicated on adult MEFs was related to an ordered system of innervation that was also reminiscent of the patterns of innervation seen at younger ages. In muscle A (Fig. 3C) the MEFs were connected by axons in a linear order that is unlikely to occur by chance ($p<0.001$). As in the newborn linear order, we found that also in the adult, the order of the neurons in the linear order was compatible with the tendency of some axons to specifically innervate, more often, fibers with larger caliber. First, the 5 motor units encompassing the thinnest muscle fibers (which was a subset of the 8 smallest motor units) did not innervate any MEF (out of the total 6 motor units which did not innervate MEFs). Second, all the motor units that showed preference to innervate small fibers (a rank sum test with $p<alpha=0.05$; 6 motor units) did not innervate any MEF (5 motor units) or were located at the periphery of the linear order (1 unit). The only units that showed preference to innervate large muscle fibers in particular were located in the center part of the linear order and were the two largest motor units (axons 3 and 5; asterisks in Fig. 3C). In muscle B (Fig. S3) the pattern of connectivity is also

highly unlikely to have occurred by chance. As already mentioned the same pairs of motor units share more than one muscle MEF. Moreover, two motor axons concentrated their innervation on MEFs to a greater degree than expected by chance: Axon 1 innervated 9 MEFs (69.23% of the 13 MEFs) and a total of 10 endplates on MEFs (38.46% of the 26 MEF endplates) ($p<0.05$). And axon 2 innervated 5 MEFs (38.46%) and a total of 7 endplates on MEFs (26.92% of the endplates) ($p<0.03$). This repeated innervation of the same endplates by a small number of 7 axons ($p<0.0045$; see MC in Methods) indicates, consistently with the linear order in muscle A and in younger ages, that the innervation pattern is structured from birth (dense connectivity) throughout maturation during the phase of massive synapse elimination and in adulthood (sparse connectivity) when some fibers still maintain multiple synapses.

This non-random connectivity implies that the MEF-innervating axons have something in common. However, we have not found evidence that there is any particular feature of the muscle fibers (other than being MEFs) that makes them a distinctive muscle fiber type. Although adult muscle fibers are organized into distinct types (both biochemically and functionally), we did not find evidence of muscle fiber properties that set these fibers apart. In particular, the caliber of the adult muscle fibers, which is a strong indicator of adult muscle fiber type (Frontera and Ochala 2015), was broad and uniformly distributed and not significantly different from the distribution of the singly innervated muscle fibers (we used bootstrapping to test whether the MEF CSAs differ in min, max, median values from a random subset of SEF fibers in the adult and all estimates were not unlikely to occur by chance; $p>0.1$ in Muscle A). At birth, MEF fibers, although thicker (higher CSA; $p<0.01$), did not have distinct sarcomere structure than SEF fibers (z-line thickness, sarcomere spacing; see Fig. S5). Moreover, the myonuclear domains on both MEFs and SEFs were not significantly different from each other. We also found that the motor units of the axons innervating endplates on MEFs (12/18 axons on muscle A and 7/16 axons on muscle B) are what we would expect to occur by chance if we account for the centrality of the muscle (mean in Muscle A 16.0833 endplates, $p>0.1$; mean in Muscle B 18.2857 endplates; see Methods). Finally, in five adult interscutaris muscles, we found no consistent incidence of muscle fibers that had multiple endplates. One adult muscle (P30) had only 3 MEFs (1.4% of the muscle fibers) and, at the other extreme, one muscle (P30) had 46 MEFs (18.1% of the muscle fibers). Such a large variability in the number and proportion of MEFs on adult muscles suggests that MEFs are not functionally essential for the proper function of the interscutularis muscle. It was therefore unlikely that these MEFs belonged to one type (see Discussion). Nonetheless it was clear (see above) that they were innervated in a non-random way.

Junction elimination on MEFs

The non-random connectivity in adult MEFs has commonalities with the patterns of innervation at earlier stages and thus provides a potential link between the developmental ordering phenomena and the ultimate adult pattern of innervation (i.e., the size principle). We wondered therefore if the simplicity of two-endplate muscle fibers could give us insights into the mechanism that foments, or in some cases prevents, synapse elimination. We already know that the newborn muscle has ~6-fold more multiple endplate muscle fibers than adult muscles (see above) thus during the period of synapse elimination there is endplate loss. We found that the tendency for endplate loss is strongly distance dependent. Although endplates at birth are sometimes near each other, none of these pairs are maintained in adults. For example, in the newborn there were 29 pairs of endplates (~37.6%) that were apart from each other by less than 50% of the width of the innervation band (the maximal distance between paired endplates on a muscle fiber, 0.975 mm). However, in adult muscles we never observed a pair of endplates on the same fiber that were closer than 50% of the extent of the innervation band (maximal distance between endplates ~1.88 mm). Rather, all the adult multiple-endplate pairs on muscles A and B were at least

0.753 mm apart (Muscle B). This distance dependence was highly significant (means differed across developmental stages; $p<0.0001$) and the distance between the closest endplates significantly increased across maturation: between P0 and all other developmental ages P10, P12, P30 and P60 (Fig. 4B; ranksum of the mean of the left side of the distribution; largest p-value $p<0.025$ between P0 and P10), and between newborn (P0) and intermediate stage (P10 and P12) ($p<0.001$), intermediate stage and adults ($p<0.02$) and newborn and adults ($p<1/10^9$). The loss of the nearby endplate pairs occurred gradually during the first weeks of postnatal life. Importantly, however, distance did not guarantee that both endplates would be maintained on the adult muscle fiber. The portion of distant endplates on multiple-endplate fibers in the newborn muscle was large. More than 20% of the fibers possess endplates that were far apart, more than half the maximal possible distance at that age. Hence, comparing this portion to the small number of multiple-endplates in adults (~6%), we estimate that most of these paired distant endplates at birth (all are at least ~0.5 mm apart) are also eliminated. Interestingly, at an intermediate age (P10) 4 nearby endplates on multiple-endplate muscle fibers were found. In each case, the same axon innervated both endplates (Fig. 4D) although in each case we anticipate that one or the other endplate will be eliminated. We also found 4 adult muscle fibers where the same axon innervated both endplates (albeit they were much further apart and presumably will be stably maintained throughout life). We therefore conclude that endplate elimination requires action at a distance: in some manner the presence of one endplate decreases the sustainability of another endplate on the same fiber, especially but not exclusively, if it is nearby. However we found no evidence that muscle fibers with one endplate ever lose that endplate, arguing that endplate elimination shares properties with intra-junctional synapse elimination in that it is a competitive process: the fate of an endplate is related to the presence and position of another endplate on the same muscle fiber. This is analogous to the fate of one axon at a multiply innervated endplate: its fate is related to the presence and position of other axons at the same junction (Turney and Lichtman 2012).

One possible mediator of action at a distance that leads to endplate elimination is the postsynaptic cell (i.e., muscle fiber) activity. We noted that during the phase of synapse elimination from individual neuromuscular junctions, endplates on MEFs became singly innervated earlier in development than those on single endplate muscle fibers (SEFs). For example, at P10, 73% of the endplates on MEFs were singly innervated whereas among endplates on SEFs a significantly smaller portion (44%) were singly innervated ($p<1/10^8$; Fig. 4C). Because synapse elimination is widely believed to be activity-dependent (W. A. Harris 1981; Stryker and Harris 1986; Meister et al. 1991; Balice-Gordon and Lichtman 1994; Personius and Balice-Gordon 2001; Wyatt and Balice-Gordon 2003), it is possible that when two endplates coexist on the same muscle fiber, the elimination process can be impacted both by intra- and inter-junctional sources of activity and hence lead to more rapid synapse elimination. We consider the possibility that this source of activity is postsynaptic action potentials (APs) traveling along the muscle fiber from one endplate to another. Several lines of evidence support the view that a propagating action potential may destabilize neuromuscular junctions and AChRs. The central tenet of this idea is that synaptic sites that are not activated by local neurotransmitter release are destabilized by depolarization from another source (e.g. blocking sites with alpha bungarotoxin (Balice-Gordon and Lichtman 1994), snake muscle multiple-endplate fibers that lack APs also have multiple endplates (Lichtman, Wilkinson, and Rich 1985) and multiple innervation of each, AP can inhibit expression of AChRs along a muscle fiber; see Discussion). But because the adult interscutalaris muscle maintains at least a few MEFs, we however need to explain why in some cases postsynaptic action potentials traveling between distant endplates can be either destabilizing or not, depending on circumstances.

Unlike intra-junctional synapse elimination which removes all but one axon, the complete loss of an endplate

removes all the axons from that site. This only occurs if an additional endplate on the fiber is maintained. In this sense the interjunctional endplate loss is competitive because the survival of one endplate is adversely affected by the presence of another on the same muscle fiber. As stated above, propagating APs could be the

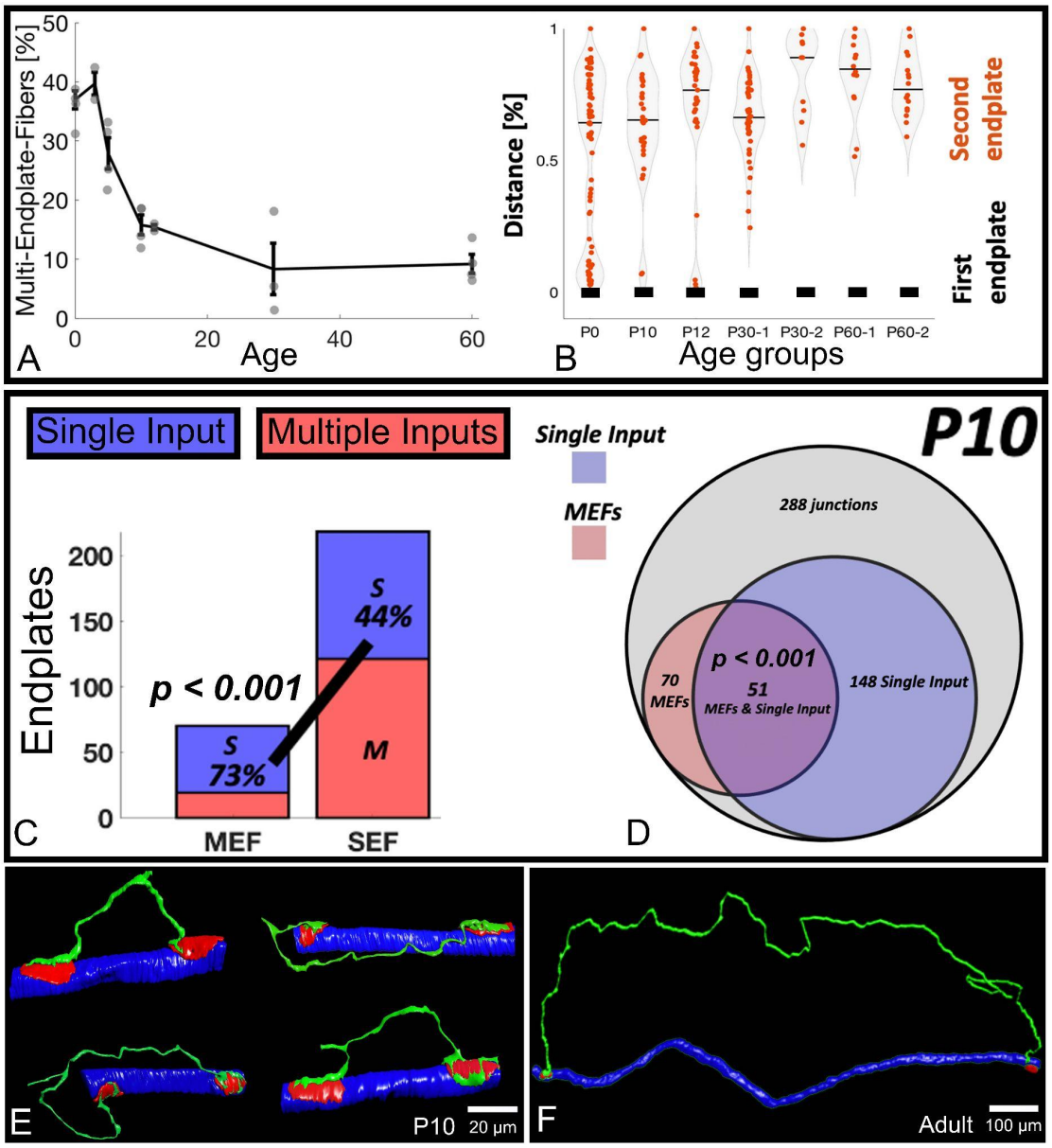

Figure 4. Action at a distance: distance dependence and axon identity dependency on the fate of elimination between paired endplates. A. Removal of excess endplates across development. **B.** Distance dependence in the elimination of excess endplates across maturation. **C-D**. In an intermediate developmental stage (P10) the endplates on multiple-endplate-fibers (MEFs) are closer to becoming singly innervated than endplates on SEFs, which are more likely to continue to be multiply innervated (C) while the conjunction of an endplate to be both on MEF and singly innervated occurs significantly more often that expected by chance (D). This suggests that synapse elimination in endplates on MEFs is more advanced than that on SEFs. **D.** The few pairs of endplates that are nearby at P10 are innervated by the same axon. The distance dependence (A-B), the faster elimination on MEFs (C-D), the mono-neuronal innervation of nearby endplates at P10 (E), the existence of an order between the axons innervating pairs of junctions on MEFs, all suggest that the existence of an additional endplate on a fiber, and the specific axons innervating the two junctions, affect the fate of additional endplates on the muscle fiber. We conjecture that collision of action potentials may be the mechanism that allows remote endplates to develop independently of each other and coexist in adulthood (F).

destabilizing factor. However, the destabilizing effect must be blocked in certain circumstances as some muscle fibers stably maintain two endplates in adulthood. One potential mechanism is the literal blockage of APs when two propagating impulses “collide” at a certain point on a muscle fiber (Bernhard Katz and Kuffler 1941; McComas, Kereshi, and Manzano 1984; Lateva, McGill, and Johanson 2002; Lateva, McGill, and Elise Johanson 2010). AP collision occurs because following the propagating depolarization is the absolute refractory repolarizing wave, in which nearly all voltage gated sodium channels are inactivated. This refractory condition prevents one AP from passing through another along an axon or more relevant here, a muscle fiber. In an attempt to better understand how multiple endplates may coexist, we calculated the conditions for an AP from one endplate to collide with the AP from another endplate on the same muscle fiber (see Table 1). Obviously, if both endplates initiate an AP at exactly the same time, the APs will certainly collide and annihilate each other midway between their origins. The broader question is: how asynchronous can the initiation of APs be and still lead to collision? The most extreme asynchrony that would still lead to collision is when one AP arrives at an endplate at the same time when the other AP generated in that endplate is in its refractory period (see discussion). To make these calculations we used previous research documenting the conduction velocity of muscle fibers and myelinated (adult) and poorly myelinated (juvenile) axons. The simplest case is when the same axon is innervating both endplates on a MEF because the axon branches to the two junctions emerge from a common branch, simplifying their relative time to reach their respective endplates. One situation where two MEFs are innervated by the same axon was already mentioned: in P10-aged animals there were MEFs with junctions that were near each other (41-72 μm) that in all cases were co-innervated by the same axon. Because none of these nearby pairs were maintained in adulthood (i.e., one or the other junction is always eliminated) we suspected that, despite being innervated by the same axon, the nerve induced APs at the two endplates did not collide. This idea was supported by the different conduction velocity delays (based on differences in length and caliber) of the two motor axon branches distal to their common branch point, and other delays associated with synaptic transmission at this developmental age (see below). For example in axon 3 in Table 1, the (presynaptic) APs may reach one endplate ~118 μs before reaching the other endplate (and 73 if we assume axonal conduction velocity near terminals of 1 m/s; see for example (B. Katz and Miledi 1965a)). However, given the estimated muscle fiber conduction velocity (based on its caliber) and the proximity of the endplates (72.3 μm), it only requires 51 μs for the AP to propagate from one endplate to the other. Thus, the first activated endplate will send an AP that will reach the other endplate before that endplate is activated. However when the second endplate is finally activated (66 μs later) it is likely that the refractory period of the AP originating at the first endplate will block its propagation. This spike-timing difference would eventually trigger the loss of the second endplate (consistent with the absence of nearby endplates on adult MEFs). In addition, two other factors may contribute to a greater desynchronization between the endplate activities. Synaptic delays (time gaps between presynaptic and postsynaptic currents) due to dynamics of quantal release (B. Katz and Miledi 1965b) vary across endplates and across repeated activation of the same endplate from 0.5 ms to 1.5 ms (mode is ~1 ms). In addition, presynaptic blockage of AP is associated with smaller caliber and thin axon branching (Krnjević and Miledi 1959). Hence, even if the two axonal branches reaching the two sufficiently nearby endplates were similar in their length and caliber, one endplate can still be activated before the other with a spike-timing difference of more than 0.5 ms. This difference allows the first endplate to send an AP that reaches the other endplate before it is activated. Hence, endplates that are separated by less than the distance of 1 ms travel of postsynaptic APs will not be stable; no collision is predicted if two endplates are separated by a 125 μm of slow-conducting muscle fiber (0.25 m/s) and even larger distances of about 750 μm for faster-conducting muscle fibers (1.5 m/s). By contrast, in adults some (but not all) of the distant endplates are still situated on muscle fibers and are not

eliminated (separated by at least 1 mm of muscle fiber). For example, for the axon in Figure 4E, the length difference between the two axonal branches reaching the two endplates on the same muscle fiber is on average 1.861 mm (2.515 +/- 0.654 mm), which corresponds to a time difference of ~ 0.1241 ms for a slow axon conduction velocity of 15 m/s. Due to this time difference, one endplate will likely be activated before the other, and the time it takes for the postsynaptic AP to propagate from the former to the latter, 2.211 mm apart on the muscle fiber, is about 1.474 ms, considerably larger than the delay (0.1241 ms) between the two presynaptic APs. This arrival time is long after the activation of the delayed endplate and hence the two APs that are produced at the two endplates will collide somewhere along the muscle fiber. Therefore, muscular APs elicited by two sufficiently synchronous endplates (relative to their distances) will collide with each other, producing no electrical effect at the endplates. Conversely, two sufficiently desynchronized endplates will affect each other via propagation of muscular APs. This dichotomy is a possible explanation for the emergence of the axonal order in the network of axon innervating fibers with multiple endplates.

DISCUSSION

The purpose of this study was to obtain a better description of the extensive re-wiring that occurs in the neuromuscular system in early postnatal life. We generated complete connectional maps at birth, at one week of age, and in adults, as well as partial maps at other stages. The hope is that this description would offer clues into the still mysterious underlying processes that lead to an orderly recruitment of motor units, known as Henneman's size principle (Henneman 1957), which, from small to large, allows each recruited axon to add a discrete tension step owing to the complete lack of co-innervation at the same neuromuscular junctions by multiple axons. This non-overlapping partitioning of muscle fibers into motor units is an emergent property of development, because at birth motor units are larger and neuromuscular junctions are co-innervated by 10 or more axons (Callaway, Soha, and Van Essen 1987; Juan C. Tapia et al. 2012). We believe that comparing wiring diagrams across ages, while painstaking, is informative because of the illuminating results from a recent longitudinal connectomic study on invertebrate development, which we participated in, that showed that fine aspects of the wiring diagram could be best understood through the lens of nervous system maturation (Witvliet et al. 2021).

We observed a number of things that were new to us. First, using serial section electron microscopy, we found that the vast majority of motor units at birth were substantially larger than any adult motor unit, and none of them was the sole input to any muscle fiber. This implies that all classes of motor neurons projecting to a muscle undergo substantial pruning. Second, despite the fact that motor units at birth were many fold larger than in adults, they ranged in size in a manner that was similar to adult motor units: there were a number of relatively small motor units, a few intermediate-size motor units, and several gigantic ones innervating about half of the muscle fibers. Third, there was a correlation between the size of the muscle fibers (cross sectional area) and the size of the motor units that provided innervation to them. This correlation between motor unit size and muscle fiber diameter was similar to the relationship between large motor units and the largest fast twitch muscle fibers in adults (Henneman and Olson 1965; Zajac and Faden 1985; Hämäläinen and Pette 1993). The identity of motor units (by size) allowed us also to realize that the cohort of axons that shared innervation at the same neuromuscular junctions was not a random subset of all the axons, but that axons of similar motor unit size tended to share muscle fibers more often than expected in a random model. All of these could have suggested that muscle fiber types were already in existence at birth and classes of axons strictly confined innervation to one

of the classes as is the case in adults. However, the tendency of axons to co-innervate particular muscle fibers, or not, appeared to be graded rather than binary. Large motor units did innervate large muscle fibers but this was a tendency not a strict rule. Moreover, the innervation preferences of axons could be ranked in a linear order such that an axon's innervation proclivities were most similar to the axons on either side of it in the linear ranking. Small motor units were close to other small motor units in the order and large motor units were near other large motor units. But because there was considerable overlap of different kinds of motor units at each neuromuscular junction the ranking was subtle to ferret out at this age (see however below). This overlap among motor units could mean that the size principle emerges by gradual pruning of axon branches to parcellate muscle fibers into smaller and smaller groups until each group is part of only one axon's motor unit (see more below). Finally, we found that many muscle fibers (>30%) possessed two or rarely three neuromuscular junction sites (endplates). Other studies have made note of multiple-endplate muscle fibers, especially in facial and neck muscles (Sandmann 1885; Agduhr 1919; Cattell 1928; Bernhard Katz and Kuffler 1941; Jarcho et al. 1952; Hunt and Kuffler 1954; Iwasaki 1957; Rossi and Cortesina 1965; Brown, Jansen, and Van Essen 1976; Bendiksen, Dahl, and Teig 1981; Zenker, Snobl, and Boetschi 1990; Duxson and Sheard 1995; Happak et al. 1997; Périé et al. 1997; Lateva, McGill, and Johanson 2002). The interscutularis muscle is also a neck muscle. Interestingly the axons that innervated the pair of neuromuscular junctions on a fiber were not identical, further suggesting that strict chemospecificity between motor axons and muscle fibers was not likely the cause of the tendencies of multiple motor units to share more muscle fibers than expected by chance which we discuss below.

At birth, the ordering of motor units was subtle because so many axons co-innervated each neuromuscular junction. At P6-9 days after birth however, when the remaining multiple innervation was mostly due to only two axons sharing the same neuromuscular junction, this ordering became more obvious. Using brainbow technology (Livet et al. 2007; Tsuriel et al. 2015) to obtain connectomes in the larger P6-9 muscles, we found a striking pattern of innervation in which axons showed a gradient of preferences that in many muscles could be arranged into a nearly perfect linear order such that the axon at one extreme shared muscle fibers mostly with the axon next in "rank" and the same axon co-innervated neuromuscular junctions progressively more rarely with axons further away in the ranking axon (see Fig. 5). Axonal interactions at sites of neuromuscular junctions were therefore akin to the interaction of neighbors along a street: most interactions occur with immediately adjacent neighbors, less so with neighbors a house away, and with progressively fewer interactions with neighbors further down the block. However, unlike a street, this linear order was abstract: it was not explained by topographic features of where the synapses were located. To the best of our ability we were unable to map the linear order to a motor map in the muscle; nearly all axons distributed their branches over much of the muscle and the center of gravity of each motor unit was not shifted in a way that could explain the ordering.

Because of the topographic variability of motor units within the same muscle in different animals ((Lu et al. 2009) and confirmed here), one attractive idea is that the linear order is an emergent property explained by the similarities or differences in neural activity patterns among the cohort of axons innervating a muscle in a more or less random fashion. Remarkably, a similar ordering of preferences motif was described by Purves and colleagues as the laws of "contiguity" and "segmental dominance" in the spinal cord innervation of ganglion cells in the rodent sympathetic chain (Lichtman, Purves, and Yip 1979, 1980). In that system, preganglionic innervation from different but overlapping sets of spinal cord segments are linearly ordered in their innervation of cohorts of ganglion cells that project to different regions of the body. In both systems no topography was evident in the location of postsynaptic cells that shared the same subsets of axons (Lichtman, Purves, and Yip 1979,

1980). Because reinnervation recapitulates the pattern of innervation the authors thought chemospecificity was the likely explanation for this pattern (Njå and Purves 1977). In muscle we do not know if the origin of the

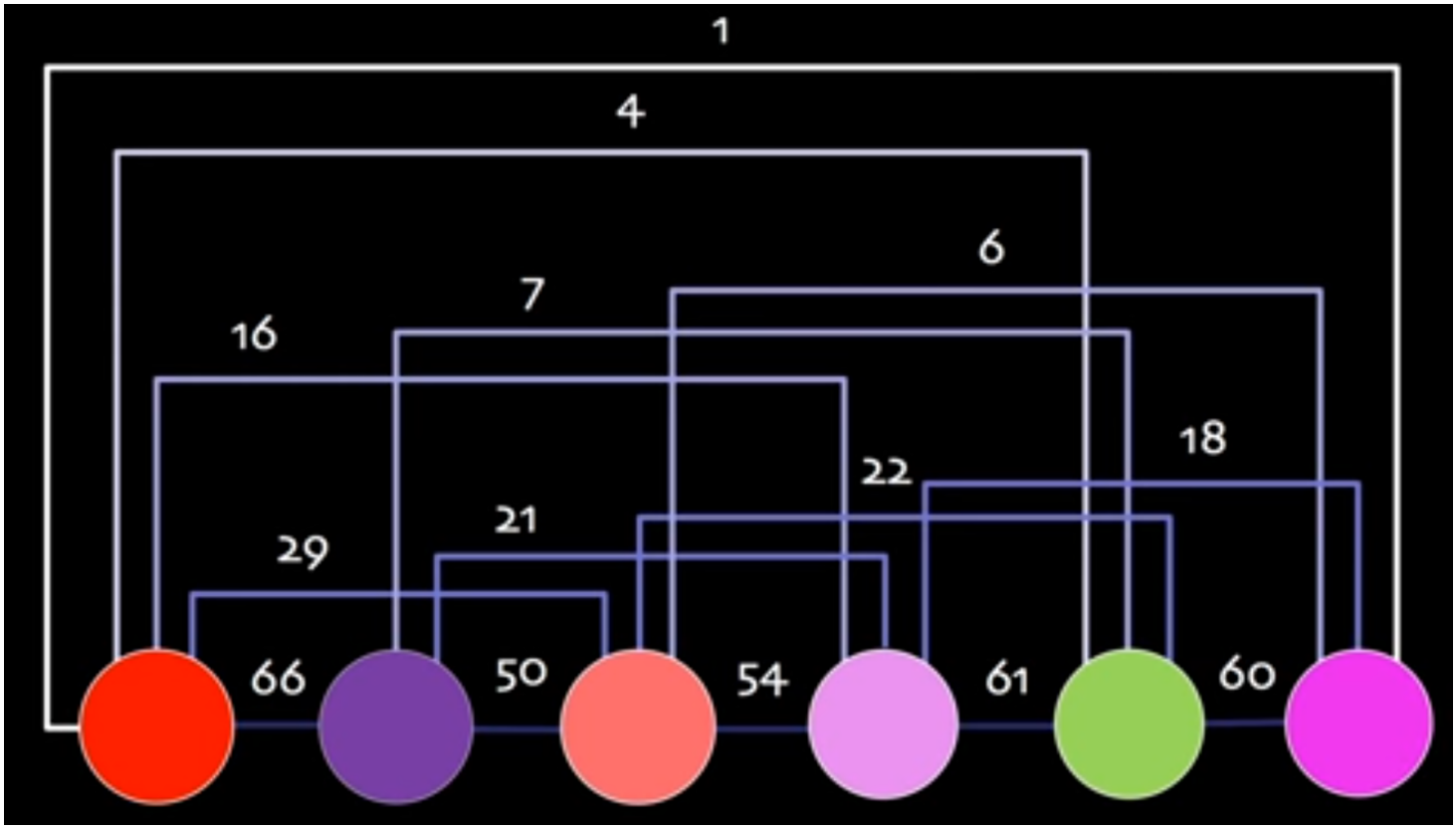

Figure 5. The linear order of connectivity at a P6 neck muscle based on brainbow labeling. This small muscle has only 6 motor units (represented by the colored circles). The number of muscle fibers co-innervated by a pair of motor neurons is given above the line connecting them. For example, the leftmost red motor unit co-innervates 66 muscle fibers with the purple motor unit, 29 muscle fibers with the salmon motor unit, 16 muscle fibers with the mauve motor unit, 4 muscle fibers with the green motor unit and only one muscle fiber with the hot pink motor unit. Such co-innervation gradient is recapitulated for each axon. Remarkably, the same order (red, purple, salmon, mauve, green, hot pink) describes the gradient of connectivities throughout the entire connectome. This order is not represented by a topographic map in the muscle.

ranking is also the position of neurons along the rostral-caudal axis of the spinal cord. Whatever its cause, its presence raises the possibility that this ordered overlapping connectivity is related to the emergence of the ordered recruitment of motor neurons in the size principle. We had assumed that making this link would be challenging, given that adult neuromuscular junctions are singly innervated, not allowing us to know which of the adult axons were sharing muscle fibers at earlier ages. But surprisingly a remnant of multiple innervation remained on a small number of adult muscle fibers in the form of the inputs to the few muscle fibers that maintained two neuromuscular junctions. These co-innervated adult muscle fibers showed preferences that were compatible with a linear order of specificity and thus provided a connection between the adult pattern of innervation and the linear order present at developmental ages.

One fundamental question is whether these preferences in muscle are based on chemical matching between motor axons and muscle fibers or rather are due to preferences based on similarities in the timing or amount of activity. There are arguments supporting each idea. As already mentioned in the adult rodent superior cervical ganglion there is a linear order of overlapping preganglionic connections among the population of postsynaptic

ganglion cells that are thought to be based on chemospecificity. This pattern is similar to the juvenile linear order in muscle. On the other hand, the decision as to which axon is the sole survivor at each muscle fiber is based on a competition that can have more than one outcome. For example in this work we noted that in most instances muscle fibers with two neuromuscular junctions ended up with different axons at each site, indicating that there is not a single motor axon that is the appropriate choice, nonetheless all adult neuromuscular junctions undergo synapse elimination until only one axon remains. A number of lines of evidence support the idea that activity differences among the innervating axons is an important determinant into which axon terminal is maintained and which are eliminated (Favero, Busetto, and Cangiano 2012; Favero, Cangiano, and Busetto 2014; Personius and Balice-Gordon 2001; Callaway, Soha, and Van Essen 1987; W. A. Harris 1981; Wyatt and Balice-Gordon 2003). This study adds a new argument for the role of activity in shaping the final pattern of connections that relates to the ultimate fate of the supernumerary neuromuscular junctions on fibers that have more than one. We found that as development proceeds the relative (and absolute) distance between neuromuscular junctions increases as the number of fibers with multiple endplates decreases. This means that neuromuscular junction elimination is less likely to occur if the junctions are far apart. Moreover the last remnant of nearby neuromuscular junctions that are present in the second postnatal week always had the same axon innervating both sites. We show that there is a plausible mechanism to explain these results based on the conduction of action potentials from one neuromuscular junction to another and the prevention of this, if the activities of the two junctions is close enough in time for the action potentials to collide as they propagate (slowly) in the muscle fiber between the 2 endplates. Thus we propose that muscle fibers that retain 2 endplates do so because the activity at the two sites is so similar that they basically have no way of communication due to action potential collision. Consistent with this view is the linear ordering of the axons that participate in the innervation of MEFs.

All of these results argue for a considerable amount of coordination in the connectivity of different axons. Unlike a strict molecular matching, the outcomes are graded and variable -- even when axons maintain synapses on the same muscle fiber they are usually not the exact same axon. Rather, a role for activity-based interaction between competing synaptic contacts seems to be regulating both synapse elimination within a neuromuscular junction and the perseverance or elimination of distant synaptic sites on MEFs. The fact that this coordination can impact synapses that are even 1 millimeter apart invites speculation about whether such mechanisms might coordinate inputs to neurons. For example synapses on the basal and special dendrites of pyramidal neurons in the cerebral cortex are separated by a long distance; however the intervening region of the cell is capable of generating back-propagated action potentials providing a system not entirely unlike a MEF. More generally we wonder if the recruitment order idea present in the neuromuscular system may provide insights into the ways other graded brain phenomena (e.g., the intensity of an emotional response) are organized. We suspect that the events that regulate which axons are eliminated and which strengthen on muscle fibers as they develop will have implications for many other parts of the nervous system.

ACKNOWLEDGEMENTS

We would like to thank the Computational Connectomics Group (CCG) of Prof. Nir Shavit at MIT CSAIL for insightful discussions on input synchronization. We would also like to thank several individuals who greatly contributed to this work. Jincheng Tian for his enormous efforts to reconstruct the muscle fibers in the newborn sample, Vikram Norton for inspiring discussions and hard work on the reconstruction of several axonal arbors, Emma Yang for multifaceted contribution to the reconstruction of the newborn sample, Sophia Laskaris for insightful discussions, animal care and preparation of the machine learning datasets for the muscle fiber

expansion and mitochondria classification, Tien Tran for axon reconstruction in the EM dataset, John Brady for assistance with manual reconstruction of axons from the EM datasets and inspiring discussions on multiple-endplate fibers early in this study, Marta Montero Crespo for insightful discussions and precious assistance with the identification and reconstruction of the endplates in the EM dataset, Marco Badwal for many discussions and his early contribution to the research, including reconstruction of the extra-muscular dataset, Siyan Zhou for help with the initial analysis of the confocal image with the EM and reconstruction of Schwann cells in the nerve, Xupeng Chen for helping with the reconstruction of part of the extra-muscular bundle and assistance with Schwann cell reconstruction.

TABLES

P10 nearby junctions

P10 MEF	CV-muscle fiber	CV-terminals	L2-L1 terminals	L mus fiber	T1 early to remote	T2 late local - terminal dependent	Collision	margin - time diff
	m/ms	Max (ms)	(μm)	(μm)	muscle dependent (ms)	fast (ms)	fast terminal	(ms)
1	1.5	0.62	19	41.3	0.028	0.031	FALSE	0.003
2	1.5	0.62	40	59.3	0.040	0.065	FALSE	0.025
3	1.5	0.62	73	72.3	0.048	0.118	FALSE	0.070
4	1.5	0.62	13	65.6	0.044	0.021	TRUE	-0.023

Table 1. Prediction of collision of postsynaptic AP in developmental multiple-endplate fibers with pairs of nearby endplates. The length (L) of the terminals to their nearby branchpoint and the length of muscle fiber between the nearby endplates (L1-L2) were estimated from the volume by reconstructing and skeletonizing the axons and muscle fibers in VAST (Berger, Seung, and Lichtman 2018). The axon conduction velocities (CV) near terminals were obtained from (B. Katz and Miledi 1965a), and see also (B. Katz and Miledi 1965b), using properties of axons of similar diameter. Due to possible differences in the cable properties between the studies, the maximal experimentally observed axon terminal CV was used (in favor of collision). We also doubled that speed to account for possible variabilities and obtained conservative predictions for AP collision. In all of these cases, the model predicts that collisions of postsynaptic action potentials will not occur at P10 (T1<T2). When collision is predicted by the model (T2<T1), it happens at the extreme end of the temporal collision window (T1-T2 close to 0) - In these cases the well-documented variability in synaptic delay (across repetitions and between endplates), often above 0.5 ms, will occasionally prevent AP collision (B. Katz and Miledi 1965b).

METHODS

Sample acquisition and preparation of the newborn sample for ssSEM

Thy1-YFP16 mice (Feng et al. 2000) were bred and housed according to the guidelines of the Harvard Animal Care and Use Committee. In newborn pups (postnatal day 0, P0), deeply anesthetized with ketamine-xylazine, the interscutularis muscle was exposed and labeled with 5 μg/ml Alexa 647-conjugated alpha-bungarotoxin (ThermoFisher Scientific, USA) for 10 minutes at room temperature to stain acetylcholine receptors as a guide for neuromuscular junctions. Immediately after thoroughly rinsing the muscle with 0.1 M phosphate-buffed saline（pH=7.4, PBS, ThermoFisher Scientific, USA), the interscutularis muscle was immersed with a solution

containing 2% glutaraldehyde (Glut., EMS, USA) and 2% paraformaldehyde (PFA, EMS, USA) in 0.1M sodium cacodylate buffer (pH=7.4) for 6 hours at 4°C. Then, under a Leica fluorescent dissecting scope (Leica, Germany), the interscutularis muscle was isolated and trimmed to only contain the entire endplate band and ~1 mm of the posterior auricular nerve. After trimming, the sample was placed directly in the concave cavity of a glass slide and immersed in 0.1 M PBS to help keep the muscle from drying. A coverslip was placed over but did not touch the sample. Then, the sample was imaged using Zeiss LSM 710 confocal microscope equipped with Plan-Neuluar 10 x 0.3 NA objective. YFP and Alexa 647 were excited by 514 nm and 633 nm lasers respectively. The purpose of confocal imaging was to capture the nerve's rough contour of innervation. It assisted further electron microscope image processing. We acquired tiled stacks of the entire endplate band scanning YFP and Alexa-647 simultaneously at a resolution of 0.923 μm, 0.923 μm and 3.017 μm for x, y and z dimensions respectively. After imaging, the sample was postfixed with 2% Glut and 2% PFA in sodium cacodylate buffer (0.1M, pH = 7.4) at 4°C for 12 hours, and processed for electron microscopy as previously (Juan Carlos Tapia et al. 2012). Briefly, the sample was contrasted with ROTO (Reduced Osmium tetroxide-Thiocarbohydrazide-Osmium tetroxide; (Juan Carlos Tapia et al. 2012) and dehydrated with graded concentrations of ethanol (20%, 50%, 70%, 80%, 90%, and 100%; 15 min each), and propylene oxide (PO, 15 min twice). Finally, the sample was immersed in a mixture of 3:1 (30 min), 1:1 (1 h), 1:3 (3 h) of PO and Plain Resin (Nisshin EM, Tokyo, Japan), and infiltrated with pure Plain Resin for 12 hours. After replacing the resin at least four times, the sample was finally embedded in beam capsules and cured in an oven at 50°C for 24 h and 70°C for 4 days.

Sample sectioning for ssSEM

The surface of the resin block was first trimmed to a rectangle, and the corners of the rectangle were then trimmed to form an arrow-point on each end of the now six-sided polygon block using a 3 mm ultratrim diamond knife (Diatome, USA) and a UC6 ultramicrotome (Leica, Germany). The fibers were spatially aligned with the length of the rectangle and sectioned perpendicular to the fiber direction in order to reduce sectioning compression. The 60 nm thick serial sections were cut with a 45° ultra diamond knife (Diatome, USA) and collected using the automated tape ultramicrotome (ATUM) system (Kasthuri et al. 2015). The sections were cut at a speed of 0.3 mm/s and collected onto carbon-coated Kapton tape. A total of 3,232 serial sections were collected. The first 2,315 sections contain muscle tissue and the nerve innervating the muscle. The following 917 sections and uncounted sections only contain the nerve and no muscle.

Wafer fabrication and mapping

The tape holding the sections was cut into strips with a razor blade between collected sections and adhered with 25.4 mm wide double-sided conductive carbon adhesive tape (Ted Pella Inc., USA) onto 4 inch diameter circular wafers (University Wafers, USA). A total of 3,232 sections were distributed across 25 wafers. To enhance the signal from cell membranes, each wafer was first plasma-treated for 30 s (operating pressure of 1 x 10-7 mb, plasma current of 15 mA) to increase its hydrophilicity, immediately stained with 4% uranyl acetate for 3 min, rinsed with ddH2O for 30 s 10 times, air-dried, stained with 3% lead citrate (Leica UltroStain II) for 3 m, rinsed and air-dried as before, stored under vacuum. Each wafer was mounted on a metal wafer holder with fiduciaries to target high-resolution imaging by multi-beam scanning electron microscope (MultiSEM 505, Zeiss). A low-resolution (3.57 μm/pixel) optical image was acquired from each wafer mounted on the wafer holder, which identified the position of each section relative to the wafer holder fiduciaries (Hayworth et al. 2014). A six-sided

polygonal region of interest (ROI) was defined and superimposed onto each section in the optical image of each wafer using the Zen software package (Zeiss Microscopy), to target high-resolution imaging using MultiSEM 505.

ssSEM image acquisition

The first 18 wafers contain the interscutularis muscle and nerve fibers innervating the muscle, and the sections on these wafers were imaged using the multi-beam SEM, which employs 61 electron beams to scan 61 overlapping rectangular regions simultaneously (Eberle et al. 2015), producing 61 image tiles. These 61 tiles form one large hexagonal image known as a multi Field of View (mFoV). Once one mFoV has been acquired, the multi-beam SEM stage moves to an adjacent site to acquire another mFOV. All images were scanned at 4 nm/pixel resolution, with a tile overlap (within mFoV) of 0.5 μm and a between-mFoV overlap of 4%. Each ROI was imaged with landing energy of 1.5 kV with each scanning beam at 570 pA, and a dwell time of 3.2 μs/pixel. Brightness and contrast for each ROI were set to maximize the dynamic range of the images acquired, by maximizing the spread of the histogram of image grey levels without clipping its tails. Prior to imaging each ROI, the multiSEM was programmed to determine the optimal focus height and stigmation settings at 'focus support points' (FSPs) within the section. If this procedure failed at more than 25% of the FSPs, then the ROI was not acquired, and the procedure was restarted with new FSPs added; failed FSPs removed or moved to other locations. Once successful at 75% or more FSPs, Delaunay triangulation was used to interpolate a topological map of the ROI, to guide the autofocus of the multiSEM during the imaging of the ROI. The last 7 wafers with sections containing only nerve fibers were imaged using a single electron beam ZEISS Sigma. The image was scanned at 4 nm/pixel resolution, with landing energy of 1.7 kV at 1 nA, and a dwell time of 200 ns per pixel.

Image Stitching and Alignment of the ssSEM sample

Stitching and alignment of the dataset presented some challenges due to the large spatial section area, the sparsity of features in many of the tiles and sections, the arc-like structure of the tissue, and the wrinkles that appear in random places throughout the sections. These issues were addressed by the techniques described below. The overall stitching and alignment was similar to Saalfeld et al. (Saalfeld et al. 2012), where each step was parallelized over image tiles and sections.

Stitching. To stitch the tiles of the sections, point correspondences were obtained between overlapping tiles, followed by an optimization process that estimates the tile position and rotation while minimizing the matching correspondences' sum of squared errors. As a first approximation, the multiSEM stage position data acquired during the imaging phase was used to estimate the tile locations. The approximate locations were used to detect overlapping areas between pairs of tiles. Next, a CLAHE filter was used to increase the contrast between these areas (e.g., in low texture regions such as blood vessels), followed by ORB (Rublee et al. 2011) features computation in each of the areas. The features of the overlapping tiles were matched in order to find correspondences. To remove outliers of incorrect correspondences, the RANSAC algorithm (Fischler and Bolles 1981) was used while optimizing for rigid transformations where the assumed rotation is less than 5 degrees. Finally, the optimization of the tiles' rotation and position that minimizes the sum of squared roots of all the correspondences was done.

3D Alignment. To align the stitched sections, coarse features were detected on each section, and matched between the sections, which were then used to guide the searches for patch matches. The matching was performed between all pairs of neighboring sections up to two sections apart. Coarse features were obtained from the original tiles, to avoid the rendering of the stitched sections. The features were detected using the

OpenCV SimpleBlobDetector ("OpenCV: cv::SimpleBlobDetector Class Reference" n.d.). The detector searches for circular dark blobs, corresponding to lipids in the tissue, which appear in the same spatial location in 4-7 consecutive adjacent sections. SIFT descriptor (Lowe 1999) was used to describe the features, and after matching the features of a pair of sections, RANSAC was used to filter out wrong matches and to find an affine transformation between the sections. Next, fine-grained patch matching at half resolution was performed. To this end, a triangular mesh was laid on the sections, 1.6x1.6 μm^2 area around each mesh vertex was cropped, followed by cross-correlation search against a transformed cropped area of the neighboring section of size 4x4 μm^2. The valid cross-correlation matches were then used as an input to a 3D elastic optimization algorithm based on prior work (Saalfeld et al. 2012), which minimizes the cross layers distance of the matches while preserving the 2D structure of the sections.

Semantic and instance segmentation of the Newborn ssSEM sample

Endplate identification

Three annotators exhaustively searched for endplates by scrolling through the volume in VAST at a low mip-level, identifying axon bundles and presynaptic vesicle-filled swellings. Three independent strategies were adopted for endplate identification: one annotator followed fibers along all their length, another annotator searched for axon terminals and a third annotator extracted candidate locations based on locations indicated by the confocal stack of the tissue stained with alpha-bungarotoxin to identify AChR sites.

Muscle fiber reconstruction

An expert annotator enumerated and seeded all myofibers that intersected the right side of the volume. This approach required to scroll through the z-axis, identify the rightmost extreme of a myofiber, name it and volumetrically segment part of the fiber to assist visual search of other myofibers. This resulted in the identification of 208 muscle fibers which were skeletonized by a second annotator. Subsequently, the remaining 32 fibers were identified by backtracking fibers after all the initially seeded fibers were completely skeletonized in the volume. This backtracking was initiated both from identified endplates that were not associated with a skeletonized fiber and by a third annotator by exhaustive search for missing fibers in the horizontal middle plane of the dataset. All of the 32 fibers that were identified in the second step were: secondary fibers that did not reach the right side of the dataset, a small number of damaged fibers (~5) or fibers at the periphery of the muscle that exited the volume at a slightly more medial point relative to the initial saturated box. An additional set of cellular structures with a topology similar to myofibers was identified as being composed of myoblasts, given the absence of sarcomere structure, their shorter extent and irregular sarcolemma. Interestingly, all the secondary fibers possessed an endplate close to the location of the endplate of the primary fibers to which they were morphologically associated (Fig. S6) as reported by (Duxson, Usson, and Harris 1989).

Volumetric instance segmentation of muscle fibers. To obtain a volumetric representation of the muscle fibers we trained a neural network to detect the sarcolemma (membrane of the muscle cells), sarcoplasm (the cytoplasm of the muscle cells), and voxels that did not correspond to any of the two categories. We then applied the neural network to the entire space using mEMbrain (Pavarino, E., Berger, D. R., Morozova, O., Drescher, B., Bidel F., Kang K., Lichtman J. W., Meirovitch Y. 2019) and obtained for each voxel affine scores for the three categories. We then used the human annotation as seeds for a 3D watershed algorithm. Pre-processing consisted of Gaussian smoothing of the probability maps. Post-processing of the 3D-expanded objects included

removal of object voxels that were far from initially annotated regions, majority voting across sections, spherical filling around annotated regions that were not expanded.

Myonuclei Reconstruction

The polynuclear nature of muscle fiber cells is thought to control transcriptional activity in segmented domains of cytoplasm surrounding such nuclei. This myonuclear domain varies between fiber types (Qaisar and Larsson 2014) and is inversely associated with the fiber's oxidative capacity (Qaisar and Larsson 2014; Van der Meer, Jaspers, and Degens 2011). Additionally, in vertebrate skeletal muscle myonuclei cluster at the muscle fiber endplates, forming aggregates of synaptic nuclei with distinctive function and morphology (Grady et al. 2005). Hence, comparing the myonuclear domains of multiple endplate fibers (MEFs) and single endplate fibers (SEFs) could provide us with insights about key differences that may exist between these types of fibers. To approximate myonuclear domain, i.e. (Volume of Fiber)/(Number of Nuclei in Fiber) in the newborn sample, we approximated it by Constant*(Fiber CSA) / (Number of Nuclei in Fiber) under the assumption that fibers maintain a relatively fixed CSA and that all fibers have similar lengths. We reconstructed all the synaptic and nonsynaptic myonuclei of 52 (25 MEFs and 27 SEFs) randomly selected muscle fibers in the newborn EM sample. In total we reconstructed 930 nuclei. To do so, one annotator placed skeleton nodes in each of the nuclei. We then trained a neural network using the software mEMbrain to classify pixels based on three classes: nucleoplasm, nuclear membrane, and pixels that do not belong to the two first categories. The output predictions of such a network were used by a second annotator, who expanded each seeded nucleus leveraging VAST's flood-filling tool and using the classified pixels as constraints. In particular, this was achieved by clicking on the nucleoplasm while the computed nucleoplasm probabilities are set as the source layer of the flood-filling algorithm in VAST. This required adapting the threshold for the filling operations based on the quality of the expansion, in order to avoid a too limited expansion (i.e., not reaching the nuclear membrane) or an expansion that would spill through the nuclear membrane to the sarcoplasm. At times this reconstruction method required human correction e.g. fixing the expansion by erasing where it had overflowed the nuclear membranes. Nevertheless, this semi-automatic procedure was several fold faster compared to the fully manual annotation of these objects. Finally, the nuclei were visualized in 3D and further analyzed.

Axon instance segmentation

Nerve. All axons were enumerated and manually skeletonized from wafer 12 to wafer 25 for over 1827 sections. This analysis identified a single fascicle containing nerve cells and Schwann cells, surrounded by perineurium tissue. Low-magnification inspection of the EM suggested no other fascicles projecting to the interscutularis muscle. To get a better idea of the number of distinct axons in this nerve, we identified and analyzed several cross sections of that nerve to the muscle for about another 1000 sections distal from the muscle (close to 200 um distal to the muscle fibers). The number of individual axonal cross sections in these slices matched the number of axons identified in the fully reconstructed nerve segment, i.e. 21 axons. The manually skeletonized axons were automatically expanded to a faithful volumetric 3D reconstruction using mEMbrain (Pavarino, E., Berger, D. R., Morozova, O., Drescher, B., Bidel F., Kang K., Lichtman J. W., Meirovitch Y. 2019) and adopting a similar approach to the fiber reconstruction, as explained above.

Axon bundles. The 21 axons identified in the nerve reconstruction were traced throughout the muscular tissue by seven annotators (three experts and four extensively trained undergraduate students). The estimated total number of annotation hours exceeded 3500 human annotation hours. The first task was to skeletonize the

axonal bundles as deeply as possible iteratively across all possible bifurcations using the annotation software VAST. Once the procedure was saturated, three annotators commenced tracing from identified endplates, connecting anonymous axon segments to identified fascicles, until all axonal branches were either associated with a synapse (the vast majority of cases) or rarely reached specialized zones containing disorganized axonal swellings surrounded by intricate glial processes close to the sarcolemma of a muscle fiber. We were unable to exclusively determine the nature of these regions with the hypothesis that they are related to sites of muscle innervation from the embryonic stage which we speculated might be associated with early stage axonal retraction from neuromuscular junctions.

Sample preparation of brainbow mice

Transgenic brainbow animals

To label motor neurons in multiple colors, we initially tried 'first generation' multicolor transgenic strategies that relied on cytoplasmic expression of fluorescent protein (Livet et al., 2007). These strategies fell short because of the limited number of distinguishable colors or low expression levels early in postnatal life. To have early onset of bright labeling in many colors, we developed new lines of Brainbow transgenic mice in which all fluorescent proteins were membrane tethered (Fig. S7). Because changes in axon caliber have a greater effect on volume than on surface area, we reasoned that the membrane label might be brighter and more uniform than the cytoplasmic label for fine neural structures at any given expression level. To create the multi-color membrane label, we generated Brainbow mice in which three fluorescent proteins (eCFP, eYFP, mCherry) were directed into the plasma membrane by an N-terminal palmitoylation tag (Kay et al., 2004). We crossed these mice to $Hb9^{cre}$ transgenic mice, which express Cre recombinase in motor neurons postmitotically (Arber et al, 1999). *In vivo* expression of the fluorescent proteins was indeed restricted to the plasma membrane. However, the fluorescent protein was localized primarily to the axon and was almost completely absent from the soma and dendrites. This compartmentalized expression likely contributed to increased brightness of motor axons.

Thy1-Membrane-Brainbow animals were generated as described (Tsuriel et al. 2015) and crossed to Hb9-Cre animals obtained from Jackson labs (JAX stock 006600).

Histology (brainbow)

Mice were deeply anesthetized with sodium pentobarbital and perfused transcardially with ice-cold 4% paraformaldehyde (Electron Microscopy Sciences) in PBS. Muscles were dissected and post-fixed in 4% paraformaldehyde for 30 min. Muscles were rinsed with 0.1 M glycine in PBS for 10 min, then 5 min in PBS and incubated for 30 min in 5 μg/μl Alexa 647-conjugated bungarotoxin (Thermo Fisher Scientific) dissolved in 1% bovine serum albumin (Sigma-Aldrich) in PBS. Muscles were rinsed again in PBS for 15 min. All post-fixation was done at 4oC, rocking in the dark. Finally, muscles were mounted on slides in Vectashield H-1000 fluorescent mounting media (Vector Laboratories), flattened with magnets overnight at -20 oC, then sealed with nail polish (Electron Microscopy Sciences), and stored in a freezer (-20oC).

To collect a sample where all axons had unique colors, we screened hundreds of animals, and analyzed muscles where the number of color redundancies among axons at the muscle entry site was limited to one or two. We always found more axon collaterals than colors at the muscle entry site. It is likely that some color redundancies were due to branching of the axon in the distal nerve (see Lu et al, 2008). In seven muscle samples the collaterals with identical colors 1) never co-innervated the same neuromuscular junction, 2) did not have motor

unit sizes twice the average size of others, and 3) displayed similar skewing in partner preferences (see below). For these reasons, these identically colored axons were likely axon collaterals rather than statistical color redundancies. Thus, these muscles contained color segmented axons that could be analyzed as complete connectomes (Fig. S8): four omohyoid muscles (P6, six axons; P7, nine axons; P7, six axons; P8, five axons) and three forepaw lumbrical muscles (P8, six axons; P9 six axons; P9, six axons).

Imaging of brainbow samples

Images were taken using the Multi-Area Time Lapse function of the Olympus FV1000 confocal microscope (Olympus Scientific Solutions Americas Corp., Waltham MA) with 3% overlap between adjoining tiles using either a 60x 1.4 NA PlanApo or 1.35 NA UPlanSApo oil immersion objective lens. The 1024x1024 and 800x800 frame size images were zoomed at 1.9 and 2.4, respectively, and stepped in Z by 0.37 μm. The 800x800 frame size was used when the image stack was greater than 121 sections due to memory limitations of the computer operating system. Samples were excited in two sequential groups to reduce spectral bleed-through: first with the 440- and 633-nm laser lines and second with the 515- and 561-nm lasers. Emission filters for four spectral channels were set as follows: Cerulean: 480/15 nm, EYFP: 535/15 nm, dTomato and mCherry: 600/25 nm, Alexa 647: long pass 650 nm. Typically the images were collected at 2 μs/pixel with either no averaging or kalman = 2.

Identification of presynaptic innervation in the confocal brainbow stacks

To assess the identity of motor axons at each junction, each image stack was individually evaluated using the 'section view' panel in the Imaris software. This panel displays a maximum intensity projection of a re-sizable subvolume of the data stack and allows real-time, user-specified gamma and threshold adjustment. By re-sizing and scrolling a small sub-volume maximum intensity projection of the data stack through the Z-dimensions, the color of each non-overlapping axonal terminal at or near the synapse could be compared to other colors present in the surrounding volume. When no non-overlapping region was available or the structure size was too small to accurately judge the color of the process, the neurite was followed back along its path to see more samples of its color and branches to which it connected. In cases where tracing was obscured by other axons of similar color or low contrast, the identity of the synapse was left "ambiguous". This occurred in less than 5% of the total junctions.

Sample preparation of YFP16 mice

Neonatal (Postnatal days 1, 3, 5, 10, 12) and Young adult *thy-1*-YFP-16 transgenic mice (P30 and P60) were anesthetized via IP (intraperitoneal injection) of 0.1ml / 20g ketamine-xylazine (Ketaset, Fort Dodge Animal Health). Following deep anesthesia, animals were transcardially perfused with 4% p-formaldehyde (PFA; Electron Microscopy Sciences, USA) in 0.1 M phosphate-buffered saline pH 7.4 (PBS; Sigma-Aldrich, USA). The interscutularis muscle, along with a ~1 mm segment of the posterior auricular nerve was dissected out, and postfixed in the fixative solution (4% PFA in 0.1M PBS, 1h). After several rinses (in PBS), samples were incubated with alpha-bungarotoxin conjugated with Alexa594 (α-btx594, 4h; Thermo Fisher Scientific) to stain the acetylcholine receptors (AChRs). Then, after removing the excess of α-btx594 with PBS (30 min, 3x), samples were mounted on slides with Vectashield mounting medium (H-1000, Vector Laboratories). In some samples, Wheat Germ Agglutinin (WGA) conjugated with Alexa647 (WGA647; ThermoFisher) was used to label muscle fibers contours, and the overall muscle vasculature. All samples were imaged using either Olympus FV1000

(Olympus Scientific Solutions Americas Corp., Waltham MA) or Zeiss LSM-710 (Carl Zeiss Microscopy, LLC, White Plains NY) confocal microscopes as indicated below.

	Day	FIBERs	NMJs	%
P0-1 (EM)	0.5	188	262	39.4
P1yfp1	1	245	341	39.2
P1yfp2	1	222	309	39.2
P1yfp4	1	234	307	31.2
P1yfp2	1	248	344	38.7
P1yfp5	1	270	368	36.3
P3-1	3	250	356	42.4
P3-2	3	230	315	37.0
P5-1	5	262	328	25.2
P5-2	5	254	334	31.5
P5-3	5	268	357	33.2
P5-4	5	254	309	21.7
P10-1	10	312	370	18.6
P10-2	10	252	287	13.9
P10-3	10	253	300	18.6
P10-4	10	252	282	11.9
P12-1	12	264	303	14.8
P12-2	12	244	283	16.0
P14				
P30-1	30	254	300	18.1
P30-2	30	205	216	5.4
P30-3	30	220	223	1.4
YFP1	60	219	233	6.4
YFP2	60	231	248	7.4

Confocal Imaging of the developmental and adult samples

We imaged whole-mounted neonatal and adult mouse muscle using Zeiss LSM-710 (Carl Zeiss Microscopy, LLC, White Plains NY) and Olympus FV1000 (Olympus Scientific Solutions Americas Corp., Waltham MA) laser scanning confocal microscope systems that were equipped with a motorized stage, high numerical aperture oil-immersion objectives (Zeiss Plan-APOCHROMAT 63x/1.4; Olympus UPlanFL N 40x/1.3 and Olympus UPlanSApo N 60x/1.35), and spectral channels to detect the fluorescence emission. The Zeiss and Olympus systems were running ZEN 2010 and FV10-ASW 4.1, respectively, and had optional software modules to manage acquisition of tiled image stacks (Zeiss: LSM StitchArt; Olympus: Multiple Area Time Lapse). We used a multi-band primary dichroic filter to reflect the laser lines needed to excite YFP, Alexa 594 and Alexa 647 (514.5nm, 561nm and 633nm, respectively). For each muscle (p1 to p60), we acquired tiled stacks of the entire

endplate band, simultaneously scanning YFP and Alexa-647 and sequentially scanning Alexa-594. The voxel size was isotropic in X, Y and Z (e.g., p1: 0.31 μm, p10: 0.42 μm and p30: 0.83 μm) to facilitate orthogonal- and off-axis slicing in subsequent analysis to count/track the mapping of endplates to muscle fibers. The Zeiss tiled datasets were montaged using the stitch function of the LSM StitchArt module. The Olympus tiled datasets were montaged in Fiji (Schindelin et al. 2012) using the Grid/Collection stitching plugin (Preibisch, Saalfeld, and Tomancak 2009). For p60 interscutularis muscle, we also imaged YFP at very high resolution on the Olympus system using the 60x objective (0.138 μm per pixel in XY and 0.2 μm in Z). The high-resolution single-channel image volume allowed tracing of the full arbor of each YFP-filled axon of the motor input (i.e., the construction of the muscle connectome when combined with the corresponding lower-resolution multi-channel image volume).

Reconstruction of muscle fibers and axon arbors and endplates from the confocal stacks

Muscle fibers, endplates, and multiple-endplate fibers. All confocal image stacks were manually annotated by two expert annotators. For the P0, P3, P5, P10, P12, P30, and P60 samples, muscle fibers were enumerated and saturated in two planes perpendicular to the muscle fiber axis at about one and two-thirds portions of the volume across the longitudinal axis of the muscle. In all samples, the respective two counts yielded the same number of muscle fibers plus or minus ~5 fibers. In P0-P5 the two estimates were averaged and used as the estimate of the number of muscle fibers in each volume. In P10, P12, P30, and P60 the muscle fibers were manually reconstructed (or in one sample automatically reconstructed using mEMbrain (Pavarino et al., 2019) and manually proofread). In all samples, the number of endplates was defined by firstly identifying potential endplates from the 3D rendering of the red (α-btx) and green (YFP16) channels of the volume in VAST, by identifying volumetric structures of a stereotypic endplate shape. At earlier ages (P0-P5), all high-energy regions with an intense red-channel signa (α-btx)l were added to the list of candidate endplates. During this process, in conjunction with careful analysis of each case, we realized that all of the identified endplates are in the vicinity of axonal bundles. We, therefore, were able to identify and skip noisy aggregation of red-channel high intensity pixels that were located far from the axonal tree. Each of the putable endplates was also analyzed by traversing the 2D image stack on transverse orientation and verifying the convexity of the perimeter of the endplate (α-btx) around the identified muscle fibers (blue-channel).

The difference between the number of identified endplates and the number of identified muscle fibers provided us with an estimate of the number of multiple-endplate fibers and their proportion in each sample. In P10-P60 we also directly classified each of the muscle fibers as multiple-endplate or single-endplate fibers by swiftly animating the 2D stack across the longitudinal axis in VAST. Both measurements gave us the same number in the vast majority of cases; when small discrepancy occurred (never more than ~5 fibers), the procedure was repeated until the source of discrepancy was identified (either an endplate was missed in the initial search for endplates from the 3D rendering, or a muscle fiber was wrongly classified during the subsequent procedure based on 2D search).

Axon tracing

Tracing the axonal arbors of two adult interscutularis muscles (P60) was accomplished in VAST (Berger, Seung, and Lichtman 2018) using manual segmentation by one expert annotator aided by a second annotator. Each annotator focused on a different part of the dataset. This was made possible due to the very high resolution YFP-based confocal images at 138 nm/pixel. The tracing strategy that we found most convenient was to trace

axons in their transverse sections which in most cases required using an orthogonal plane annotation plane in VAST. When tracing became difficult (rarely in these high-quality stacks), to avoid ambiguity, the two annotators raised concerns and attempted to reconcile contradicting opinions. Several regions required postponing the decision for a difficult axonal tracing until the companion axons, at the vicinity of the ubiquitous axon reconstruction, were reconstructed. In all cases, this led to an agreeable solution.

Statistical Tools and Analysis

Linear order of axons

Whether the innervation of muscle fibers by motor neurons is initially unspecific (random in nature) or specific (subpopulations of axons have greater tendency to innervate sub-populations of fibers) has been a topic of a number of theoretical studies (Willshaw 1981). The main tenet has been that while the fate of synapse elimination in each neuromuscular junction should depend on a combination of various functions, the cohort of axons innervating each junction likely reflects developmental factors. For example, the opportunity to innervate a junction by a specific axon may be related to the limited axon topography at a developmental time, and possibly also to the status of innervation of nearby junctions. Wilshaw specifically hypothesized that the motor system is benefiting from a random innervation pattern that is purposefully excessive at birth, only to allow each junction a sufficiently high probability to maintain at least one input (Willshaw 1981).

We assessed the level of randomness in the innervation pattern by computing for each pair of axons the probability to observe a certain number of shared muscle fiber targets, under the null hypothesis that axons are equally likely to dispense their terminals at all junctions. Indeed, in the newborn interscutularis muscle all axons, except one, are arborized at birth across the entire longitudinal axis of the muscle. All axons also innervated endplates in more or less equal numbers at the muscle regions distal and proximal to the entry point to the muscle tissue. Nonetheless, it is clear that even if endplates are innervated at equal likelihoods, the probability to innervate one endplate is not independent of the probability to innervate other endplates (the mutual information is not zero). Hence, we devised a tool to assess the global innervation pattern based on the deviations of pairs of axons from the null hypothesis that for an axon with K muscle fiber targets, all subsets of K targets are equally likely to occur.

We defined the link between two axons based on how excessive the number of targets shared between them is compared to a random innervation model. Formally, we considered for two axons with N1 and N2 targets the probability to observe exactly S shared targets assuming there exist M equally likely innervation sites.

Pshare(S) = P[axons with N1 and N2 targets share exactly S targets | M possible targets]

We then summed the probabilities to observe the actual number of shared targets or beyond.

Pshare = Pshare(S) + Pshare(S+1)+,...+Pshare(M)

This yielded a network of probabilities among all pairs of motor axons. For example, axons 17, 19, and 21 assumed a sub-network as depicted in Fig. 6. Of the 240 muscle fiber targets in the muscle, axon 17 innervated 93 fibers (innervation ratio ~39%) and axon 21 innervated 90 fibers (innervation ratio ~38%). If their muscle fiber targets are innervated with equal likelihood and independently of each other, we would expect that one axon will

innervate the targets of the second axon with the same ratio of innervation as it innervates the entire muscle. However, we found that the number of shared targets, 54, is ~58% and ~60% of the number of muscle fiber targets innervated by the two axons, respectively. The probability to observe this number of shared targets, or more, for motor unit sizes 93 and 90, and for a total of 240 possible targets, assuming independence of innervation, is about 387/10^10 (Wang, Zhao, and Zhang 2015). As we do not assume that the probabilities to innervate two junctions are independent of each other, we will use the above probability Pshare as a score for the tendency of two axons to innervate many targets. This can be seen as a way to deal with the number of shared muscle fiber targets of two axons with a normalization for the prior (fixed from the data) for the number of targets of each axon, and the total number of available targets.

Similarly, we also compute the probability Pavoid by considering the number of targets that are not innervated by each axon and the number of targets that are jointly not innervated by the two axons (the complement of the overlap and motor unit sizes).

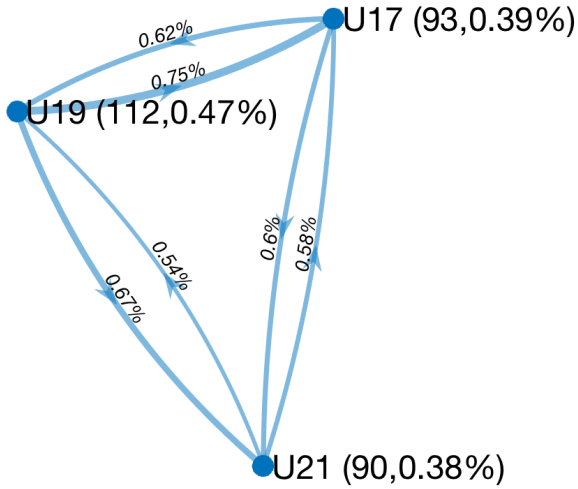

Figure 6. Co-innervation diagram of three motor units. Each node represents one motor unit and signed edges represent the portion of the targets of a motor unit explained by the paired motor unit. Assuming 240 possible targets we calculate the probability to observe the number of shared targets under the assumption that targets are picked uniformly at random.

We were interested to see if the tendency of axons to innervate the same targets or avoid innervating the same targets is part of a global regularity of axonal networks. To this end, we defined the Sharing-network as a weighted graph of N axonal nodes, and edge weights between all pairs of axonal nodes defined by the negative log probabilities to observe the data (i.e., -log(Pshae), (Wang, Zhao, and Zhang 2015)). The larger the weight, the less likely it was to observe the number of shared targets (or more) by chance. Similarly, we build a network Avoidance-network to assess the tendency of axons to avoid innervating the same targets. When depicting these networks we observed an unexpected graph regularity which, except for one extremely sparse connectome, appeared in all the developmental ages for which complete connectomes were obtained in our data (P0 n=1; P6-P9, n=7; and P60, n=2). The regularity was shown as a tendency of axons to regularly innervate the same targets forming a special form of axonal neighborhood, with a linear appearance ($axon_1$, $axon_2$, …,$axon_K$) or in one of the adults even simpler many axons clustered together repeatedly innervating the same set of multiple-endplate fibers. To capture this regularity and assess its statistical significance, we measured the

wellness of embedding the axonal network on a line such that nearby axons share a large tendency to share the same targets (the weight from the Sharing-network) and a small tendency to avoid targets (the weight from the Avoidance-network). To do so, we first computed a 2-dimensional embedding with a spring-force algorithm that attempts to position the axons in the plane while respecting their pairwise innervation pattern (Force algorithm). We then measured the linearity of this embedding using the ratio of variances along the main axes of the embedding, formally the ratio of the first and second eigenvectors of the covariance matrices of the optimized positions.

Comparison of the empirical connectomes to graph distributions

If not stated explicitly otherwise, all the statistical assessments were carried out by comparing the developmental connectomes to theoretical graph distributions. This allowed us to derive the probability to observe the data (or more severe case) under the (null) assumption that developmental connectomes share properties with random graphs. This approach was undertaken when a permutation test that considers alternative assignments for a specific connectome (connectivity matrix) would not have been fruitful in assessing the statistics. We considered three main graph distributions.

Most commonly we used the configuration model where graphs are derived by considering a fixed number of nodes (usually for axons and muscle fibers) and edges represent the connections between them. In the asymptotic approach, to draw a graph instance from a distribution, we toss a coin with a positive probability that is proportional to the fixed degrees of the node in the data (Britton, Deijfen, and Martin-Löf 2006). In this approach, we consider a family of connectomes whose average node degree (i.e., number of connections incident to a node) is identical to the node degree in the data (e.g. number of synapses in a connectome or the number of shared targets between two axons in a co-innervation network). This approach is suitable when our biological assumption is that the number of edges (most often synaptic connections) may assume a considerable variability if many biological samples were derived. This was the case in the newborn connectome where also within the sample some muscle fibers were innervated by three axons and some by fifteen axons, and some axons innervate 13 muscle fibers and some innervate 120 muscle fibers. We do not wish to restrict the analysis to connectomes that identically follow the motor unit sizes and convergence numbers as in the data. This approach was used to produce random connectomes on which the linear order property was computed.

For the developmental ages and for the adult, allowing the variability in node degrees of the above will consider networks that are biologically irrelevant. For example, having a distribution that in average produces node degrees of one and two edges per node in the adult connectomes will allow for specific instances random connectomes with 3-4 inputs (with non negligible probability) - we however prefer to consider cases that are more consistent with what we expect may happen across samples. Hence, for these ages we used a shuffling approach that produces connectomes with exactly the same motor unit sizes and convergent numbers on fibers (or on endplates) as in the data. Also on these graphs we computed the relevant graph properties and derived the estimated p values (whose confidence intervals are known as well), including the linear order of the induced network of co-innervating axons.

In some cases where the developmental connectome assumed a special property we were interested to test some graph properties against random connectomes that have that special property and against such graphs that do not have that property (for example the connectome of the adult Muscle B which was highly central). In such cases we computed both probabilities (against different hypotheses) and described the outcomes under the

different assumptions. For example when we assessed the motor unit sizes occurring on the adult muscle B we first discovered that the motor unit sizes of axons innervating multiple-endplate fibers in that sample is larger than what occurs in random graphs of exactly the same configuration (node degrees). However, when we parsed the distribution according to the sub-distribution of networks with centrality as in muscle B that phenomenon was no longer unlikely - hence we cannot exclude the possibility that centrality in that muscle is the cause for the appearance of large motor units innervating the multiple-endplate fibers, and in fact such large motor unit sizes can be explained from the centrality alone. In other cases the specific permutation tests or parametric tests are explained in the text next to the result.

SUPPLEMENTARY INFORMATION

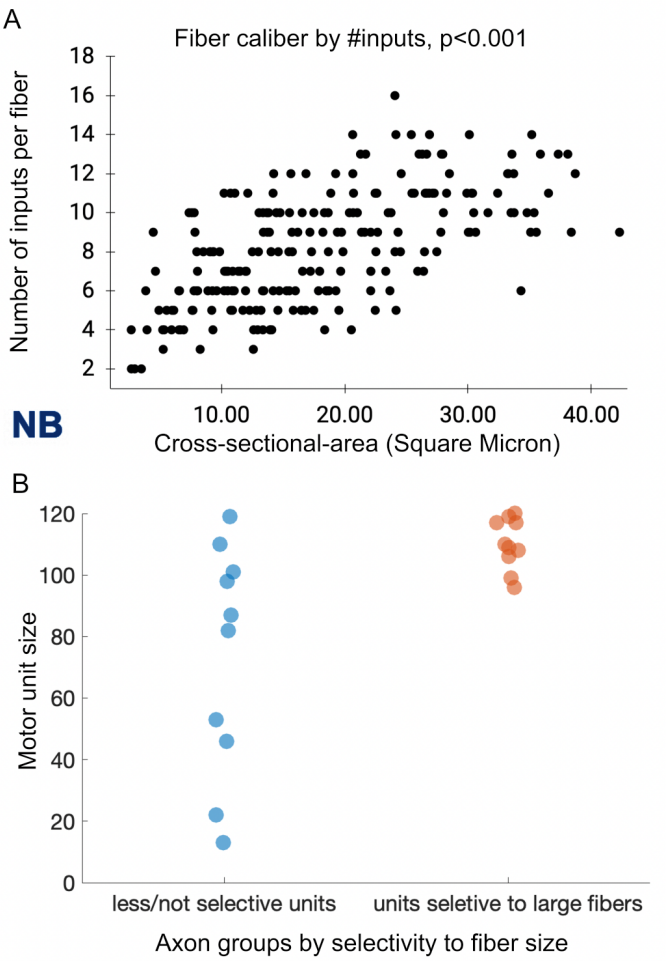

Figure S1. Association between muscle fiber size, number of inputs and motor unit size in the newborn. A. A correlation between cross-sectional area of muscle fibers and the number of distinct axons innervating them. **B.** Half of the motor units (n=10) were selectively innervating large muscle fiber targets (p<0.01); none of the small motor units was selective to large fibers and ~half of the non-selective units were large motor units (comparable in size to the selective units).

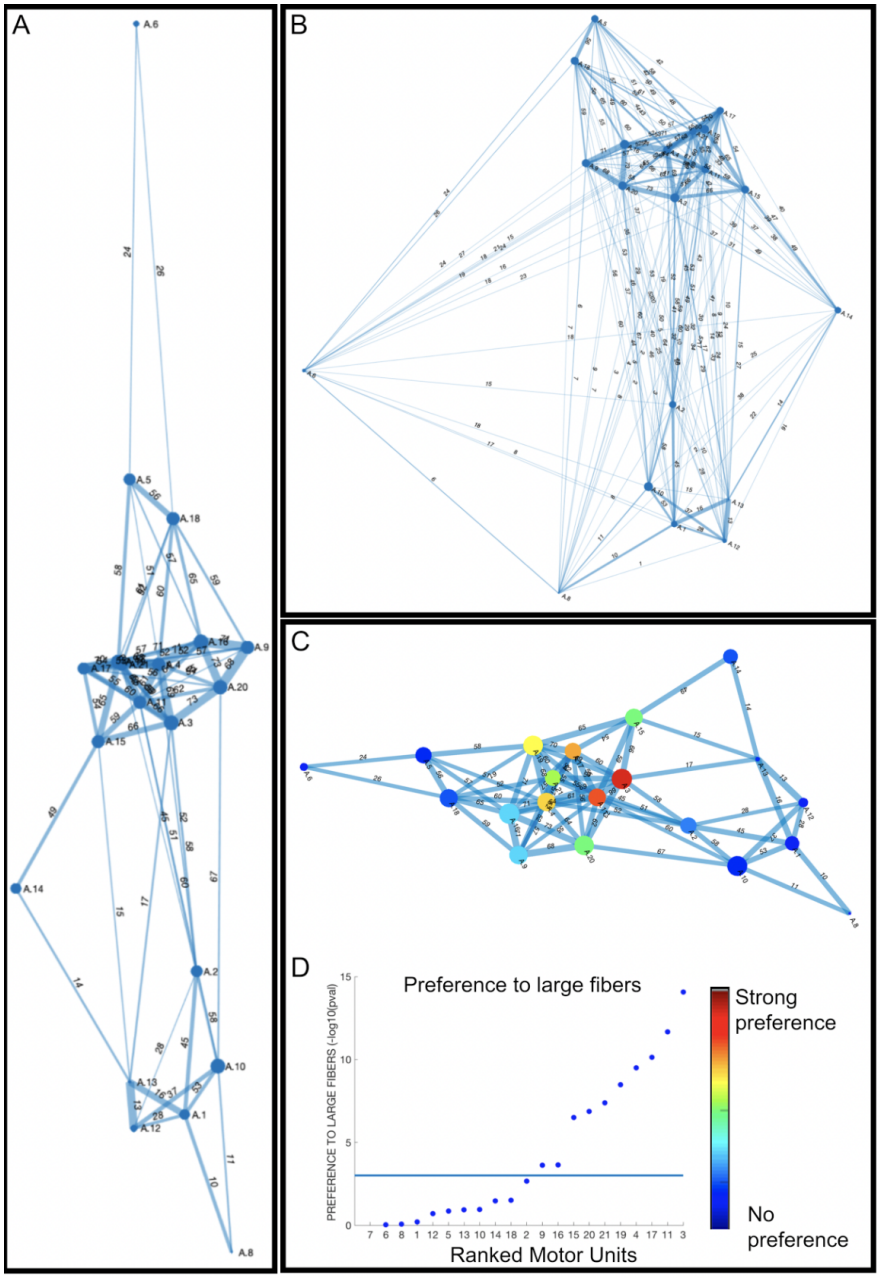

Figure S2. Representations of linear orders in the newborn. A. The linear order was computed by including only edges with p<alpha=0.01. This representation is meaningful in connectomes with sufficient statistical power to detect trends across many pairs of neurons as in the newborn sample. **B.** The pruned linear order (A) is embedded in the complete linear order as weak edges contribute little to the embedding. Both A and B are elongated embeddings among networks of random connectomes (p<0.05). **C**. Weighting the edges as a sublinear function of -log(probability) also produces linear connectome but with less elongation compared to linear weighting (A,B). **C-D.** Ranking units based on their preference to innervate large fibers reveals that the linear order is organized according to peripheries that show no preference to large muscle fibers and a central cluster with motor units that are highly selective to large muscle fibers. This suggests that the newborn linear order is consistent with the structural properties of the muscle fibers. Moreover, even when a large motor unit, such as motor unit 10, is not selective to muscle fiber size, it is still part of the periphery of the linear order.

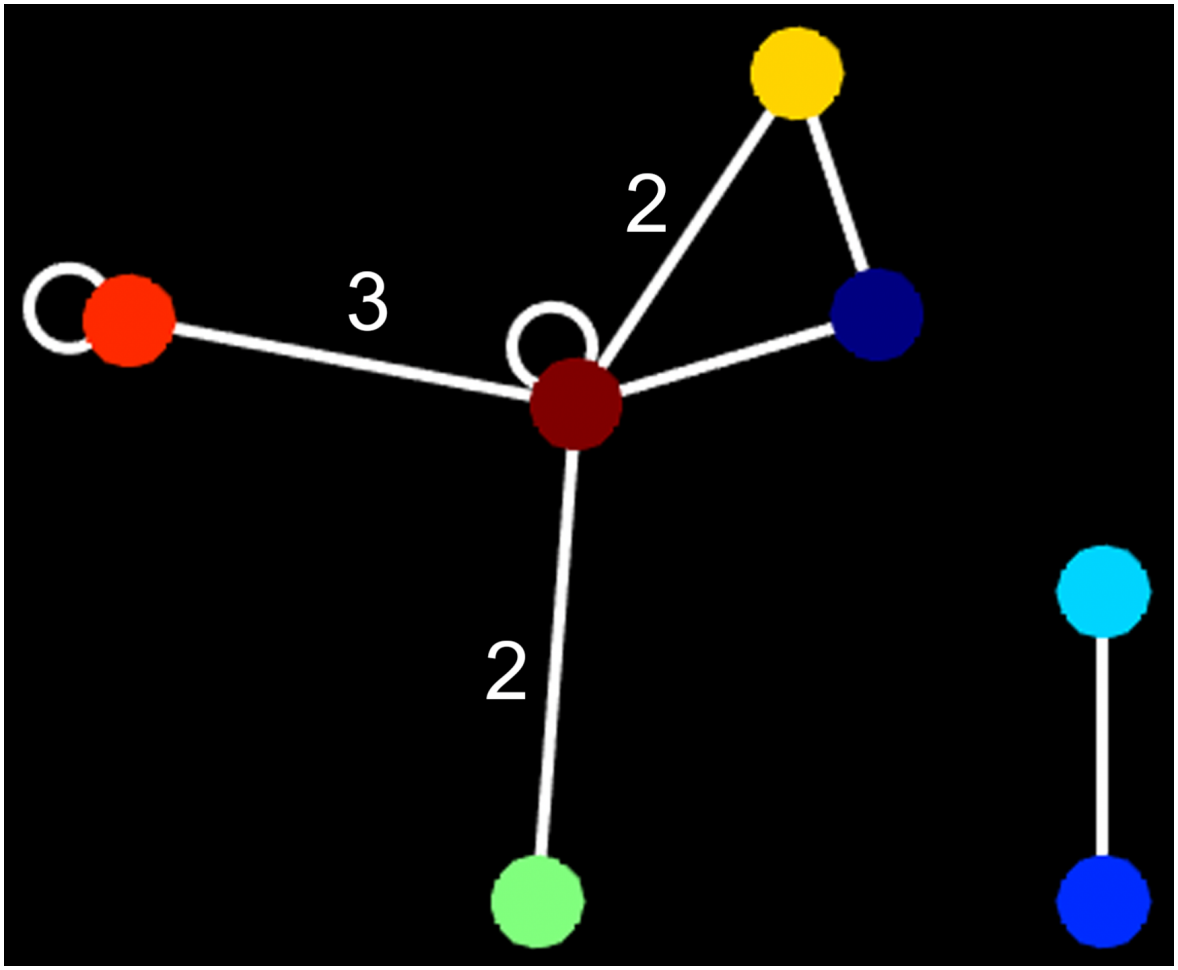

Figure S3. Clustered Innervation on multiple-endplate fibers in the Connectome of adult muscle B. Seven motor units innervated 26 endplates; too few motor units to have occurred by chance ($p<0.0045$). A pair of motor units co-innervated three multiple-endplate muscle fibers and two other pairs of motor units each innervated a pair of multiple-endplate muscle fibers.

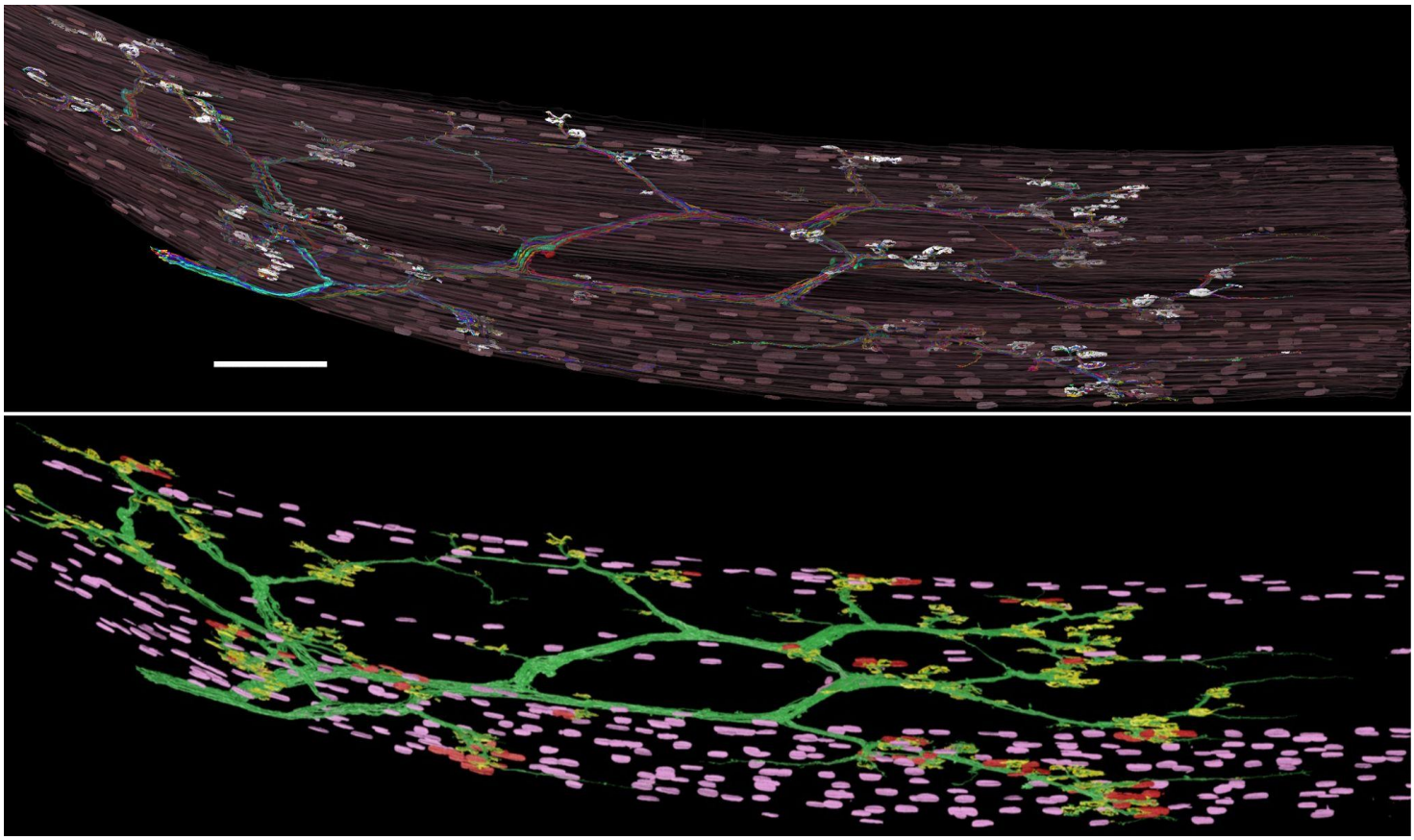

Figure S4. Saturation of all myonuclei in a subset of fibers. Top. All the synaptic and nonsynaptic myonuclei of 52 randomly selected muscle fibers in the newborn sample (25 MEFs and 27 SEFs), rendered with the axonal arbor, endplates and muscle fibers (top). **Bottom.** For each muscle fiber the synaptic nuclei (red) were identified in the vicinity of the endplates (yellow). The myonuclear domain of the MEFs and SEFs, which is indicative of oxidative capacity of fibers, and the number of synaptic nuclei, (Qaisar and Larsson 2014; Van der Meer, Jaspers, and Degens 2011), were not significantly different between the two muscle fiber groups.

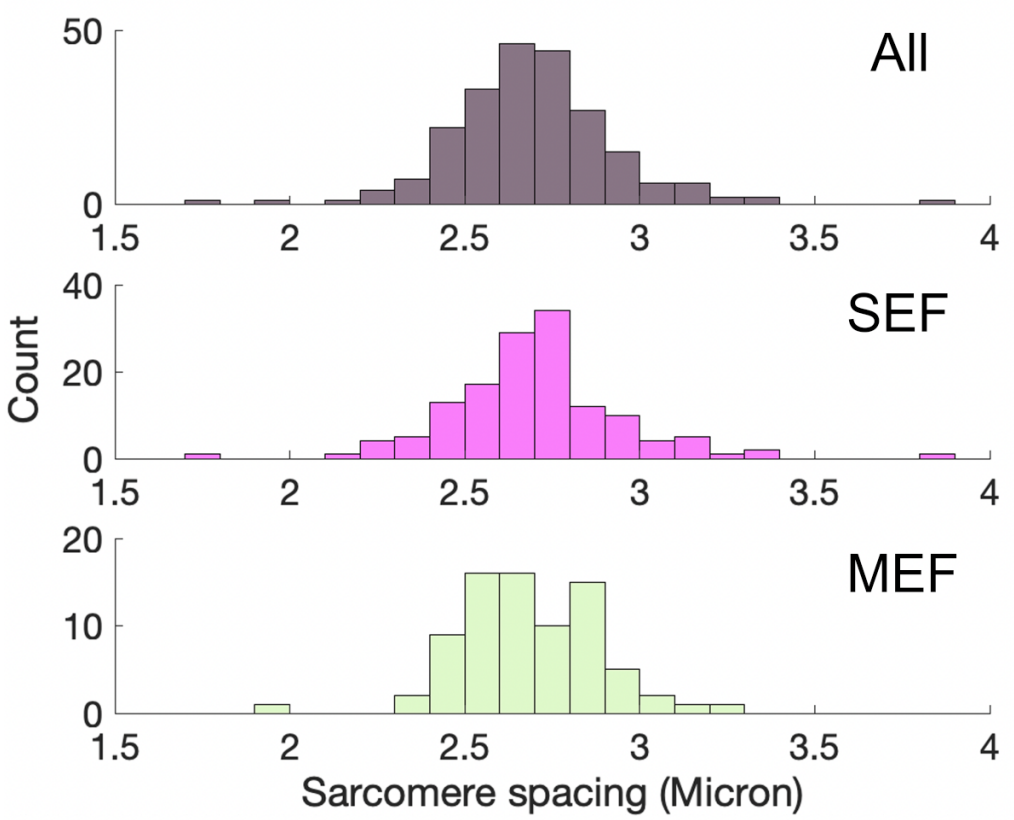

Figure S5. Sarcomere spacing in the newborn sample. The distribution of sarcomere spacing is unimodal and not distinctly distributed for the multiple-endplate (MEFs) and single-endplate (SEFs) fibers.

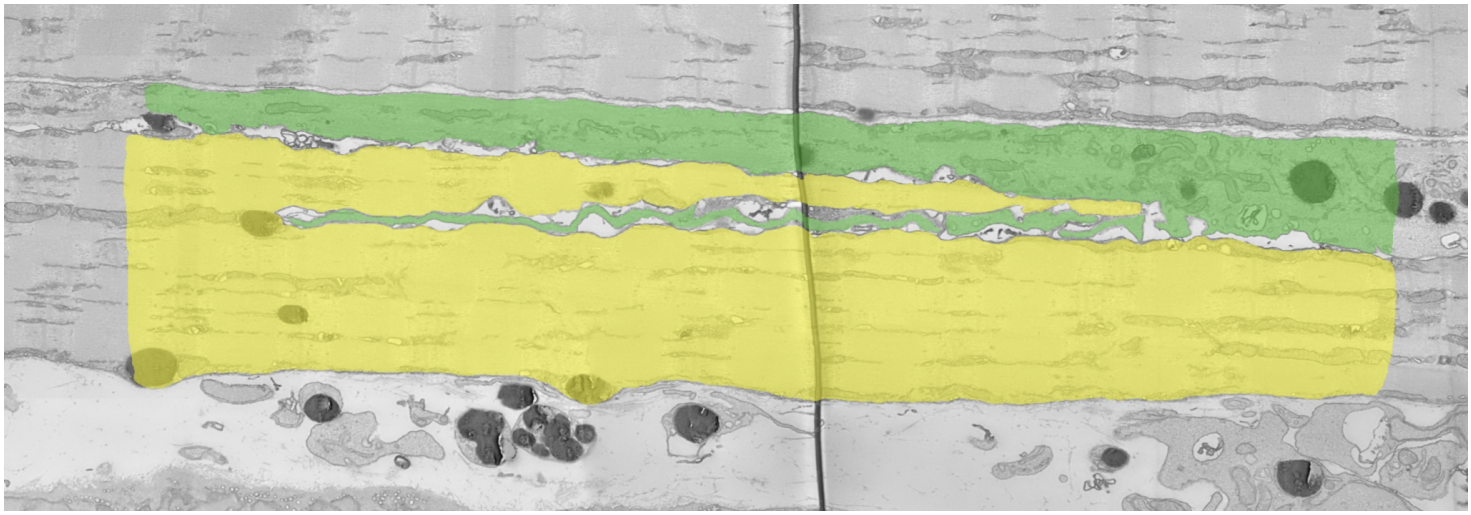

Figure S6. Primary and secondary fibers. In the newborn dataset we found several secondary fibers with immature contractile properties that were attached to other more mature primary fibers. In all cases the secondary fiber possessed endplates near the location of endplates on the primary fibers, as reported by (Duxson, Usson, and Harris 1989).

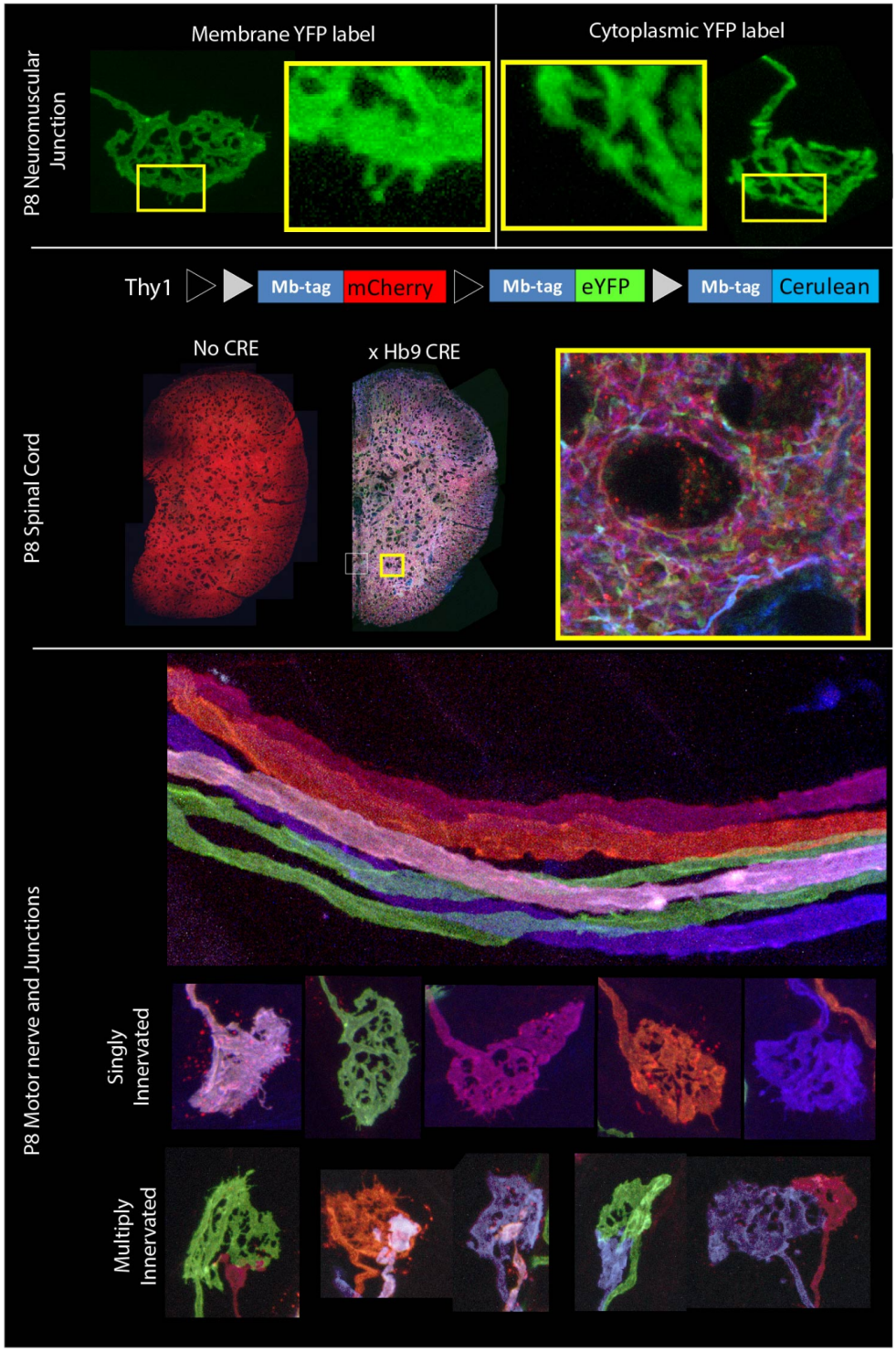

Figure S7. Membrane-brainbow expression in developing motor neurons. The top panel shows a schematic of the Brainbow 1.0 type construct. Black and grey triangles indicate Lox P and 2272 sites, respectively. Blue boxes indicate the palmitolyation membrane tag (Mb-tag). The middle panel shows expression of the construct in the spinal cord with and without Cre co-expression. Yellow box shows a high resolution image of spinal cord neuropil. Bottom panel shows all the motor axons innervating a P9 Omohyiod muscle. Five unique

colors and six axon collaterals are easily identifiable. Below are neuromuscular junctions from the same muscle, both singly and multiply innervated.

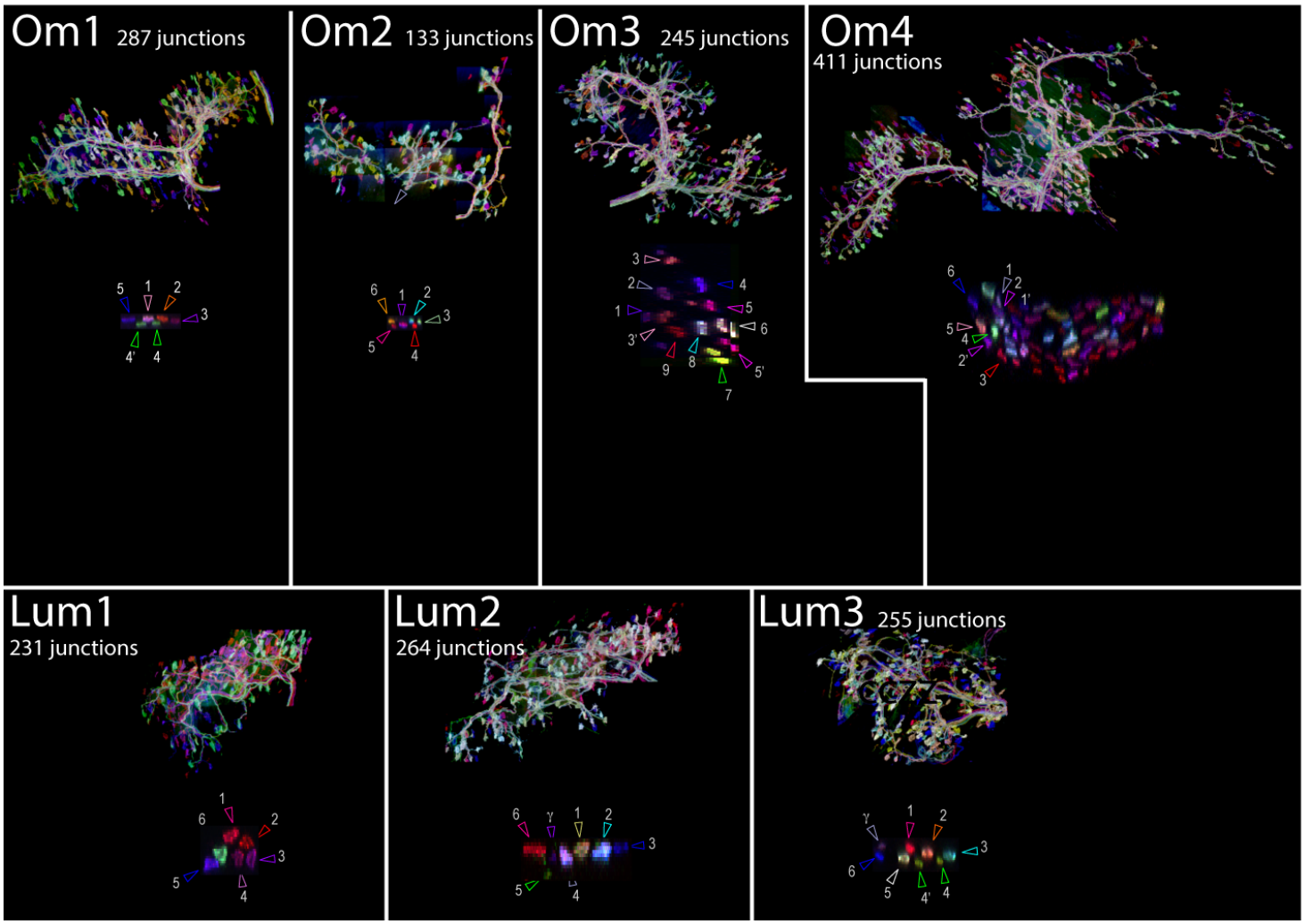

Figure S8. High resolution confocal image montages of brainbow labeled P6-9 Omohyiod and Lumbrical muscles. Each panel shows a downsized maximum intensity projection of a high-resolution, four channel three-dimensional image montage that contains all the motor axons and neuromuscular junctions in a developing muscle. Cross sections of the nerve at the muscle entry point are shown, and arrows identify the axons innervating the muscle. A sample of neuromuscular junctions are shown, one belonging to each distinctly colored axon.

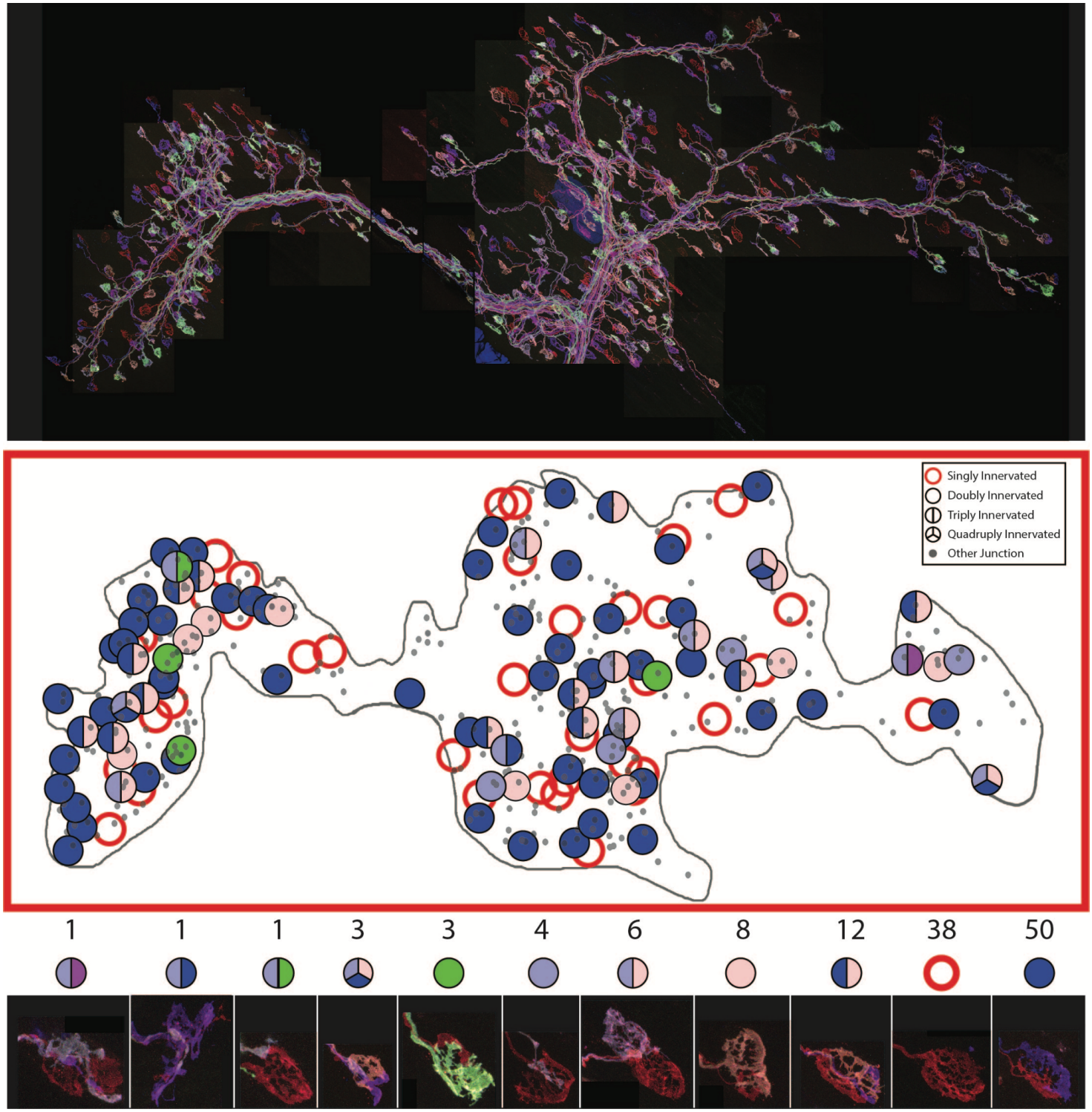

Figure S9. A map of all axon terminals for one developing motor axon. Top panel shows the maximum intensity projection of a P6 Omohyoid muscle. The identity of all axon terminals was determined based on color. The locations of all endplates are shown as small grey dots. The locations of endplates innervated by the red-colored axon are shown as large colored circles. The color of the circles indicates the identity of other axons innervating the same endplate. The bottom panel shows images of each category of endplate as well as the numbers of endplates in each category.

REFERENCES

Agduhr, E. 1919. “Are the Cross-Striated Muscle Fibers of the Extremities Also Innervated Sympathetically.” *Proc Kon Akad Wet Amsterdam* 21: 1231–37.

Balice-Gordon, Rita J., and Jeff W. Lichtman. 1994. “Long-Term Synapse Loss Induced by Focal Blockade of Postsynaptlc Receptors.” *Nature* 372 (6506): 519–24.

Bendiksen, F. S., H. A. Dahl, and E. Teig. 1981. “Innervation Pattern of Different Types of Muscle Fibres in the Human Thyroarytenoid Muscle.” *Acta Oto-Laryngologica* 91 (5-6): 391–97.

Bennett, M. R. 1983. “Development of Neuromuscular Synapses.” *Physiological Reviews* 63 (3): 915–1048.

Bennett, M. R., and A. G. Pettigrew. 1974. “The Formation of Synapses in Striated Muscle during Development.” *The Journal of Physiology*. https://doi.org/10.1113/jphysiol.1974.sp010670.

Berger, Daniel R., H. Sebastian Seung, and Jeff W. Lichtman. 2018. “VAST (Volume Annotation and Segmentation Tool): Efficient Manual and Semi-Automatic Labeling of Large 3D Image Stacks.” *Frontiers in Neural Circuits* 12 (October): 88.

Britton, Tom, Maria Deijfen, and Anders Martin-Löf. 2006. “Generating Simple Random Graphs with Prescribed Degree Distribution.” *Journal of Statistical Physics* 124 (6): 1377–97.

Brown, M. C., J. K. Jansen, and D. Van Essen. 1976. “Polyneuronal Innervation of Skeletal Muscle in New-Born Rats and Its Elimination during Maturation.” *The Journal of Physiology* 261 (2): 387–422.

Buffelli, Mario, Giuseppe Busetto, Lorenzo Cangiano, and Alberto Cangiano. 2002. “Perinatal Switch from Synchronous to Asynchronous Activity of Motoneurons: Link with Synapse Elimination.” *Proceedings of the National Academy of Sciences of the United States of America* 99 (20): 13200–205.

Burke, R. E., D. N. Levine, and F. E. Zajac 3rd. 1971. “Mammalian Motor Units: Physiological-Histochemical Correlation in Three Types in Cat Gastrocnemius.” *Science* 174 (4010): 709–12.

Callaway, E. M., J. M. Soha, and D. C. Van Essen. 1987. “Competition Favouring Inactive over Active Motor Neurons during Synapse Elimination.” *Nature* 328 (6129): 422–26.

Cattell, M. 1928. “Plurisegmental Innervation in the Frog.” *The Journal of Physiology* 66 (4): 431–42.

Duxson, M. J., and P. W. Sheard. 1995. “Formation of New Myotubes Occurs Exclusively at the Multiple Innervation Zones of an Embryonic Large Muscle.” *Developmental Dynamics: An Official Publication of the American Association of Anatomists* 204 (4): 391–405.

Duxson, M. J., Y. Usson, and A. J. Harris. 1989. “The Origin of Secondary Myotubes in Mammalian Skeletal Muscles: Ultrastructural Studies.” *Development* 107 (4): 743–50.

Eberle, A. L., S. Mikula, R. Schalek, J. Lichtman, M. L. Knothe Tate, and D. Zeidler. 2015. “High-Resolution, High-Throughput Imaging with a Multibeam Scanning Electron Microscope.” *Journal of Microscopy* 259 (2): 114–20.

Favero, Morgana, Giuseppe Busetto, and Alberto Cangiano. 2012. “Spike Timing Plays a Key Role in Synapse Elimination at the Neuromuscular Junction.” *Proceedings of the National Academy of Sciences of the United States of America* 109 (25): E1667–75.

Favero, Morgana, Alberto Cangiano, and Giuseppe Busetto. 2014. “Hebb-Based Rules of Neural Plasticity: Are They Ubiquitously Important for the Refinement of Synaptic Connections in Development?” *The Neuroscientist: A Review Journal Bringing Neurobiology, Neurology and Psychiatry* 20 (1): 8–14.

Feng, G., R. H. Mellor, M. Bernstein, C. Keller-Peck, Q. T. Nguyen, M. Wallace, J. M. Nerbonne, J. W. Lichtman, and J. R. Sanes. 2000. “Imaging Neuronal Subsets in Transgenic Mice Expressing Multiple Spectral Variants of GFP.” *Neuron* 28 (1): 41–51.

Fischler, Martin A., and Robert C. Bolles. 1981. “Random Sample Consensus: A Paradigm for Model Fitting with Applications to Image Analysis and Automated Cartography.” *Communications of the ACM* 24 (6): 381–95.

Frontera, Walter R., and Julien Ochala. 2015. “Skeletal Muscle: A Brief Review of Structure and Function.” *Calcified Tissue International* 96 (3): 183–95.

Fruchterman, Thomas M. J., and Edward M. Reingold. 1991. “Graph Drawing by Force-Directed Placement.” *Software: Practice & Experience* 21 (11): 1129–64.

Grady, R. Mark, Daniel A. Starr, Gail L. Ackerman, Joshua R. Sanes, and Min Han. 2005. “Syne Proteins Anchor Muscle Nuclei at the Neuromuscular Junction.” *Proceedings of the National Academy of Sciences of the United States of America* 102 (12): 4359–64.

Granzier, H. L., H. A. Akster, and H. E. Ter Keurs. 1991. “Effect of Thin Filament Length on the Force-Sarcomere Length Relation of Skeletal Muscle.” *The American Journal of Physiology* 260 (5 Pt 1): C1060–70.

Hall, Z. W., and J. R. Sanes. 1993. “Synaptic Structure and Development: The Neuromuscular Junction.” *Cell* 72 Suppl (January): 99–121.

Hämäläinen, N., and D. Pette. 1993. “The Histochemical Profiles of Fast Fiber Types IIB, IID, and IIA in Skeletal Muscles of Mouse, Rat, and Rabbit.” *The Journal of Histochemistry and Cytochemistry: Official Journal of the Histochemistry Society* 41 (5): 733–43.

Happak, W., J. Liu, G. Burggasser, A. Flowers, H. Gruber, and G. Freilinger. 1997. “Human Facial Muscles: Dimensions, Motor Endplate Distribution, and Presence of Muscle Fibers with Multiple Motor Endplates.” *The Anatomical Record* 249 (2): 276–84.

Harris, A. J., and C. D. McCaig. 1983. “Embryonic Proliferation of Autonomic Axons Following Muscle Denervation.” *Neuroscience Letters* 11: S47.

Harris, W. A. 1981. “Neural Activity and Development.” *Annual Review of Physiology* 43: 689–710.

Hayworth, Kenneth J., Josh L. Morgan, Richard Schalek, Daniel R. Berger, David G. C. Hildebrand, and Jeff W. Lichtman. 2014. “Imaging ATUM Ultrathin Section Libraries with WaferMapper: A Multi-Scale Approach to EM Reconstruction of Neural Circuits.” *Frontiers in Neural Circuits* 8 (June): 68.

Henneman, E. 1957. “Relation between Size of Neurons and Their Susceptibility to Discharge.” *Science* 126 (3287): 1345–47.

Henneman, E., and C. B. Olson. 1965. “RELATIONS BETWEEN STRUCTURE AND FUNCTION IN THE DESIGN OF SKELETAL MUSCLES.” *Journal of Neurophysiology* 28 (May): 581–98.

Hunt, C. C., and S. W. Kuffler. 1954. “Motor Innervation of Skeletal Muscle: Multiple Innervation of Individual Muscle Fibres and Motor Unit Function.” *The Journal of Physiology* 126 (2): 293–303.

Iwasaki, S. 1957. “Mononeuronal Double Innervation of an Amphibian Striated Muscle Fibre.” *The Japanese Journal of Physiology* 7 (4): 267–75.

Jarcho, L. W., C. Eyzaguirre, B. Berman, and J. L. Lilienthal Jr. 1952. “Spread of Excitation in Skeletal Muscle; Some Factors Contributing to the Form of the Electromyogram.” *The American Journal of Physiology* 168 (2): 446–57.

Kasthuri, Narayanan, Kenneth Jeffrey Hayworth, Daniel Raimund Berger, Richard Lee Schalek, José Angel Conchello, Seymour Knowles-Barley, Dongil Lee, et al. 2015. “Saturated Reconstruction of a Volume of Neocortex.” *Cell* 162 (3): 648–61.

Katz, Bernhard, and Stephen W. Kuffler. 1941. “Multiple Motor Innervation of the Frog’s Sartorius Muscle.” *Journal of Neurophysiology* 4 (3): 209–23.

Katz, B., and R. Miledi. 1965a. “PROPAGATION OF ELECTRIC ACTIVITY IN MOTOR NERVE TERMINALS.” *Proceedings of the Royal Society of London. Series B, Containing Papers of a Biological Character. Royal Society* 161 (February): 453–82.

———. 1965b. “THE MEASUREMENT OF SYNAPTIC DELAY, AND THE TIME COURSE OF ACETYLCHOLINE RELEASE AT THE NEUROMUSCULAR JUNCTION.” *Proceedings of the Royal Society of London. Series B, Containing Papers of a Biological Character. Royal Society* 161 (February): 483–95.

Krnjević, K., and R. Miledi. 1959. “Presynaptic Failure of Neuromuscular Propagation in Rats.” *The Journal of Physiology*. https://doi.org/10.1113/jphysiol.1959.sp006321.

Lateva, Zoia C., Kevin C. McGill, and M. Elise Johanson. 2010. “The Innervation and Organization of Motor Units in a Series-Fibered Human Muscle: The Brachioradialis.” *Journal of Applied Physiology*. https://doi.org/10.1152/japplphysiol.01163.2009.

Lateva, Zoia C., Kevin C. McGill, and M. Elise Johanson. 2002. “Electrophysiological Evidence of Adult Human Skeletal Muscle Fibres with Multiple Endplates and Polyneuronal Innervation.” *The Journal of Physiology* 544 (2): 549–65.

Lichtman, J. W., D. Purves, and J. W. Yip. 1979. “On the Purpose of Selective Innervation of Guinea-Pig Superior Cervical Ganglion Cells.” *The Journal of Physiology* 292 (July): 69–84.

———. 1980. “Innervation of Sympathetic Neurones in the Guinea-Pig Thoracic Chain.” *The Journal of Physiology* 298 (1): 285–99.
Lichtman, J. W., R. S. Wilkinson, and M. M. Rich. 1985. “Multiple Innervation of Tonic Endplates Revealed by Activity-Dependent Uptake of Fluorescent Probes.” *Nature* 314 (6009): 357–59.
Livet, Jean, Tamily A. Weissman, Hyuno Kang, Ryan W. Draft, Ju Lu, Robyn A. Bennis, Joshua R. Sanes, and Jeff W. Lichtman. 2007. “Transgenic Strategies for Combinatorial Expression of Fluorescent Proteins in the Nervous System.” *Nature* 450 (7166): 56–62.
Lowe, D. G. 1999. “Object Recognition from Local Scale-Invariant Features.” In *Proceedings of the Seventh IEEE International Conference on Computer Vision*, 2:1150–57 vol.2. ieeexplore.ieee.org.
Lu, Ju, Juan Carlos Tapia, Olivia L. White, and Jeff W. Lichtman. 2009. “The Interscutularis Muscle Connectome.” *PLoS Biology*. https://doi.org/10.1371/journal.pbio.1000032.
McComas, A. J., S. Kereshi, and G. Manzano. 1984. “Multiple Innervation of Human Muscle Fibers.” *Journal of the Neurological Sciences* 64 (1): 55–64.
Meister, M., R. O. Wong, D. A. Baylor, and C. J. Shatz. 1991. “Synchronous Bursts of Action Potentials in Ganglion Cells of the Developing Mammalian Retina.” *Science* 252 (5008): 939–43.
Morgan, Josh Lyskowski, Daniel Raimund Berger, Arthur Willis Wetzel, and Jeff William Lichtman. 2016. “The Fuzzy Logic of Network Connectivity in Mouse Visual Thalamus.” *Cell* 165 (1): 192–206.
Newman, Mark. 2018. *Networks*. Oxford University Press.
Njå, A., and D. Purves. 1977. “Specific Innervation of Guinea-Pig Superior Cervical Ganglion Cells by Preganglionic Fibres Arising from Different Levels of the Spinal Cord.” *The Journal of Physiology* 264 (2): 565–83.
Pavarino, E., Berger, D. R., Morozova, O., Drescher, B., Bidel F., Kang K., Lichtman J. W., Meirovitch Y. 2019. “mEMbrain: An Interactive Deep Learning Tool for Labeling and Instance Segmentation.” Presented at the Bernstein Conference for Computational Neuroscience , Berlin.
Périé, S., J. L. St Guily, P. Callard, and A. Sebille. 1997. “Innervation of Adult Human Laryngeal Muscle Fibers.” *Journal of the Neurological Sciences* 149 (1): 81–86.
Personius, K. E., and R. J. Balice-Gordon. 2001. “Loss of Correlated Motor Neuron Activity during Synaptic Competition at Developing Neuromuscular Synapses.” *Neuron* 31 (3): 395–408.
Preibisch, Stephan, Stephan Saalfeld, and Pavel Tomancak. 2009. “Globally Optimal Stitching of Tiled 3D Microscopic Image Acquisitions.” *Bioinformatics* 25 (11): 1463–65.
Purves, D., and J. W. Lichtman. 1980. “Elimination of Synapses in the Developing Nervous System.” *Science* 210 (4466): 153–57.
Qaisar, R., and L. Larsson. 2014. “What Determines Myonuclear Domain Size?” *Indian Journal of Physiology and Pharmacology* 58 (1): 1–12.
Redfern, P. A. 1970. “Neuromuscular Transmission in New-Born Rats.” *The Journal of Physiology* 209 (3): 701–9.
Rossi, G., and G. Cortesina. 1965. “MORPHOLOGICAL STUDY OF THE LARYNGEAL MUSCLES IN MAN. INSERTIONS AND COURSES OF THE MUSCLE FIBRES, MOTOR END-PLATES AND PROPRIOCEPTORS.” *Acta Oto-Laryngologica* 59 (June): 575–92.
Rublee, Ethan, Vincent Rabaud, Kurt Konolige, and Gary Bradski. 2011. “ORB: An Efficient Alternative to SIFT or SURF.” In *2011 International Conference on Computer Vision*, 2564–71.
Saalfeld, Stephan, Richard Fetter, Albert Cardona, and Pavel Tomancak. 2012. “Elastic Volume Reconstruction from Series of Ultra-Thin Microscopy Sections.” *Nature Methods* 9 (7): 717–20.
Sandmann, G. 1885. “Ueber Die Vertheilung Der Motorischen Nervenendapparate in Den Quergestreiften Muskeln Der Wirbelthiere.” *Virchows Archiv Fur Pathologische Anatomie Und Physiologie Und Fur Klinische Medizin*, 240–52.
Sanes, J. R., and J. W. Lichtman. 1999. “Development of the Vertebrate Neuromuscular Junction.” *Annual Review of Neuroscience* 22: 389–442.
———. 2001. “Induction, Assembly, Maturation and Maintenance of a Postsynaptic Apparatus.” *Nature Reviews. Neuroscience* 2 (11): 791–805.
Schindelin, Johannes, Ignacio Arganda-Carreras, Erwin Frise, Verena Kaynig, Mark Longair, Tobias Pietzsch,

Stephan Preibisch, et al. 2012. “Fiji: An Open-Source Platform for Biological-Image Analysis.” *Nature Methods* 9 (7): 676–82.
Stryker, M. P., and W. A. Harris. 1986. “Binocular Impulse Blockade Prevents the Formation of Ocular Dominance Columns in Cat Visual Cortex.” *The Journal of Neuroscience: The Official Journal of the Society for Neuroscience* 6 (8): 2117–33.
Tapia, Juan Carlos, Narayanan Kasthuri, Kenneth J. Hayworth, Richard Schalek, Jeff W. Lichtman, Stephen J. Smith, and Joann Buchanan. 2012. “High-Contrast En Bloc Staining of Neuronal Tissue for Field Emission Scanning Electron Microscopy.” *Nature Protocols* 7 (2): 193–206.
Tapia, Juan C., John D. Wylie, Narayanan Kasthuri, Kenneth J. Hayworth, Richard Schalek, Daniel R. Berger, Cristina Guatimosim, H. Sebastian Seung, and Jeff W. Lichtman. 2012. “Pervasive Synaptic Branch Removal in the Mammalian Neuromuscular System at Birth.” *Neuron* 74 (5): 816–29.
Tseng, B. S., C. E. Kasper, and V. R. Edgerton. 1994. “Cytoplasm-to-Myonucleus Ratios and Succinate Dehydrogenase Activities in Adult Rat Slow and Fast Muscle Fibers.” *Cell and Tissue Research* 275 (1): 39–49.
Tsuriel, Shlomo, Sagi Gudes, Ryan W. Draft, Alexander M. Binshtok, and Jeff W. Lichtman. 2015. “Multispectral Labeling Technique to Map Many Neighboring Axonal Projections in the Same Tissue.” *Nature Methods* 12 (6): 547–52.
Turney, Stephen G., and Jeff W. Lichtman. 2012. “Reversing the Outcome of Synapse Elimination at Developing Neuromuscular Junctions in Vivo: Evidence for Synaptic Competition and Its Mechanism.” *PLoS Biology* 10 (6): e1001352.
Van der Meer, S. F. T., R. T. Jaspers, and H. Degens. 2011. “Is the Myonuclear Domain Size Fixed?” *Journal of Musculoskeletal & Neuronal Interactions* 11 (4): 286–97.
Wang, Minghui, Yongzhong Zhao, and Bin Zhang. 2015. “Efficient Test and Visualization of Multi-Set Intersections.” *Scientific Reports* 5 (November): 16923.
Willshaw, D. J. 1981. “The Establishment and the Subsequent Elimination of Polyneuronal Innervation of Developing Muscle: Theoretical Considerations.” *Proceedings of the Royal Society of London. Series B, Containing Papers of a Biological Character. Royal Society* 212 (1187): 233–52.
Witvliet, Daniel, Ben Mulcahy, James K. Mitchell, Yaron Meirovitch, Daniel R. Berger, Yuelong Wu, Yufang Liu, et al. 2021. “Connectomes across Development Reveal Principles of Brain Maturation.” *Nature* 596 (7871): 257–61.
Wyatt, Ryan M., and Rita J. Balice-Gordon. 2003. “Activity-Dependent Elimination of Neuromuscular Synapses.” *Journal of Neurocytology* 32 (5-8): 777–94.
Zajac, F. E., and J. S. Faden. 1985. “Relationship among Recruitment Order, Axonal Conduction Velocity, and Muscle-Unit Properties of Type-Identified Motor Units in Cat Plantaris Muscle.” *Journal of Neurophysiology* 53 (5): 1303–22.
Zenker, W., D. Snobl, and R. Boetschi. 1990. “Multifocal Innervation and Muscle Length.” *Anatomy and Embryology* 182 (3): 273–83.